STUDY OF THERMALLY INDUCED HIGHER ORDER MICROCANTILEVER MODES

by

ASHWINI KADAM

A DISSERTATION

Submitted in partial fulfillment of the requirements
for the degree of Doctor of Philosophy
in
The Materials Science Program
to
The School of Graduate Studies
of
The University of Alabama in Huntsville

HUNTSVILLE, ALABAMA

2006

In presenting this dissertation in partial fulfillment of the requirements for a doctoral degree from The University of Alabama in Huntsville, I agree that the Library of this University shall make it freely available for inspection. I further agree that permission for extensive copying for scholarly purposes may be granted by my advisor or, in his/her absence, by the Director of the Program or the Dean of the School of Graduate Studies. It is also understood that due recognition shall be given to me and to The University of Alabama in Huntsville in any scholarly use which may be made of any material in this dissertation.

_____ _____

(student signature) (date)

DISSERTATION APPROVAL FORM

Submitted by Ashwini Kadam in partial fulfillment of the requirements for the degree of Doctor of Philosophy in Materials Science and accepted on behalf of the Faculty of the School of Graduate Studies by the dissertation committee.

We, the undersigned members of the Graduate Faculty of The University of Alabama in Huntsville, certify that we have advised and/or supervised the candidate on the work described in this dissertation. We further certify that we have reviewed the dissertation manuscript and approve it in partial fulfillment of the requirements of the degree of Doctor of Philosophy in Optical Science & Engineering.

_____ Committee Chair

_____

_____

_____

_____

_____

_____ Program Director

_____ College Dean

_____ Graduate Dean

ABSTRACT
School of Graduate Studies
The University of Alabama in Huntsville

Degree Doctor of Philosophy Program Materials Science Program

Name of Candidate Ashwini Kadam

Title Study of Thermally Induced Higher Order Microcantilever Modes

Microcantilevers have been widely studied for sensing tiny quantities of chemical and biological analytes in both vapor and liquid media. They have been shown to respond to changes in chemical, biological, thermal and physical processes. The primary sensing mechanisms are static bending due to induced differential surface stress and changes in the fundamental resonant frequency upon mass uptake. Although the possibility of using thermally induced higher order modes has been suggested for sensing and for understanding the mechanical behavior of microcantilevers, experimental demonstrations have not been given in the literature. Studies of thermally induced spectra provide an alternate in-situ detection technique for microcantilever sensing that is attractive in that no external excitation mechanism is required. However, thermally induced higher order modes have smaller amplitudes than what is obtained with external excitation.

This dissertation examines the use of thermally induced higher order microcantilever modes both for sensing and studying adsorption induced interfacial changes between the Au coated microcantilever surface and Hg. The use of a thermally

induced spectrum takes advantage of the fact that no additional external components are necessary to study them when using the optical lever (AFM style) detection technique.

A process to microfabricate rectangular microcantilevers is optimized and demonstrated. Thermally induced higher order flexural modes are demonstrated for Hg sensing with Au coated microcantilevers. Furthermore Hg sensing is carried out with microcantilevers having different Au coverage to investigate the use of thermally induced higher order modes for sensing. Two different types of Au surfaces are employed for Hg sensing with microcantilevers, one obtained by thermally evaporating Au, and the other by sputtering Au. Although the conventionally used deflection signal showed a similar trend to Hg with both these films, exactly the opposite spectral response was observed. It is shown that the local stress variations due to the adsorption induced surface changes can be sensitively detected with higher order modes rather than conventional deflection monitoring. Microcantilevers have also been fabricated using SU-8 (an epoxy based polymer) to check if the thermally induced spectral response of these flexible (Young's modulus: 5 GPa) microcantilevers can show improvement in the spectral sensing response. Hg studies of the SU-8 microcantilevers experimentally support that the mode frequency, and not the mode order, is responsible for the observed greater sensing response of the higher order modes.

Abstract Approval: Committee Chair _____
(Date)

Department Chair _____

Graduate Dean _____

ACKNOWLEDGMENTS

I would like to thank my advisor, Dr. Gregory Nordin, for his invaluable guidance, encouragement, and support throughout the entire process of this work. I thank Dr. Michael George for being the committee chair. I would also like to thank the members of my committee for their helpful comments. I am grateful to the students and staff at the Nano and Micro Devices Center and Laboratory for Materials and Surface Science for the useful discussion. I would also like to thank everyone who has directly or indirectly helped to make this work possible.

Finally, I would like to give very special thanks to my husband, Rajesh and son Shantanu. Without their constant understanding, love and support none of this would have been possible.

TABLE OF CONTENTS

Page

LIST OF FIGURES

LIST OF TABLES

LIST OF SYMBOLS

Symbol	Definition
Q	Quality factor associated with a vibrational mode
k_B	Botlzman constant
f_n	Frequency of n^{th} order mode
T	Absolute temperature
L	Microcantilever length
w	Microcantilever width
t , h	Microcantilever thickness
ρ	Density of the microcantilever material
ω_n	Angular frequency of microcantilever vibration
E	Young's modulus of microcantilever material
α_n	A constant for n^{th} order mode
n	Mode order
m^*	Effective microcantilever mass
k	Spring constant of microcantilever
m_b	Mass of the microcantilever beam
n	Geometric factor
δm^*	Change in effective microcantilever mass
δk	Change in effective microcantilever spring constant

s	Surface stress
δs	Change in microcantilever surface stress
t_i	Thickness of i^{th} layer of microcantilever

Chapter 1

INTRODUCTION

In the beginning of the 1970's, technologies generated from the microelectronics industry started to be used for fabrication of mechanical systems, so called mico electro-mechanical systems (MEMS) [1]. Since then, micrometer scale mechanical systems have been explored for a variety of applications. New techniques to improve the MEMS device response have resulted in an avalanche of publications in recent years. MEMS devices can not only be used for applied science applications but also to understand basic physics behind different phenomena.

1.1 Microcantilever Based Sensors

One of the most flexible mechanical sensor system is the cantilever sensor [2,3]. The main feature of a cantilever based sensor is transducing the mechanical behavior of the cantilever into a measurable signal, where the mechanical properties are altered by physical changes in the environment. Cantilever based sensors have a wide range of applications. Cantilevers have been demonstrated in such applications as temperature, pressure, force, chemical and biological sensors [4-13]. The two types of operation modes of a cantilever based sensor are static and dynamic modes. In the static mode the bending of the cantilever is used to transduce the desired physical quantity to a measurable signal. In the dynamic mode the cantilever's resonant behavior is used, where

shifts in the resonant frequency and the damping of the cantilever transduce the physical quantities.

One of the first cantilever based sensors is the atomic force microscope (AFM), invented by Binning et al. in 1986 [14]. In AFM, a tip is integrated at the apex of a cantilever and forces acting on the tip are transduced using the static or dynamic mode [15, 16]. In the static mode AFM, the tip is typically in contact with the surface and by scanning the cantilever across the surface and measuring the bending of the cantilever, the topography of the surface is obtained. In the dynamic mode, the tip is not in full contact with the surface and the resonant frequency shift due to the atomic forces acting on the tip serves as a measurement of the surface topography. Force sensitivities down to 10^{-10} N are routinely achieved [16].

1.1.1 Static Mode Sensors

The chemical or biological species induces stress upon interaction with the sensitized cantilever surface and hence causes bending of the cantilever. In this case the whole cantilever surface acts as the sensor and not just the tip at the cantilever apex as in AFM. A schematic drawing of the principle can be seen Figure 1.1 where in (a) the cantilever is stress free and in (b) bending is induced by molecular interaction. Several examples of surface stress sensors have been demonstrated and typically a surface stress of 10^{-5}N/m can be detected [17].

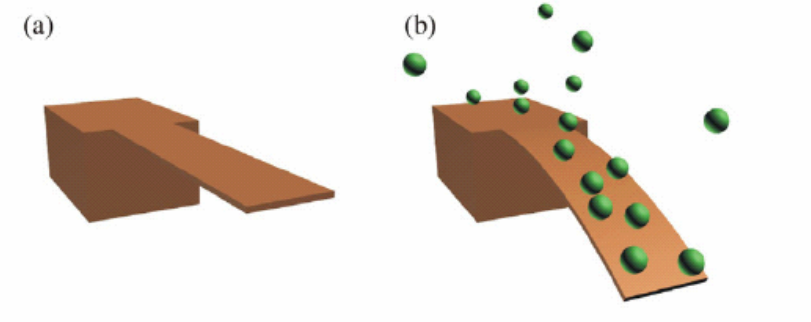

Figure 1.1 (a) A stress free cantilever and (b) molecules have interacted on the surface inducing surface stress and bending the cantilever

Several sensing studies with cantilever use change in surface stress principle. For example, Thundat et al. [18] report on a cantilever coated with an ultra-violet cross-linking polymer used as a sensitive optical UV-radiation dosimeter. When exposed to radiation, the polymer coated cantilever bends due to stress obtained in the cross-linked polymer film.

Detection of alcohols in gas has been performed by coating a cantilever with a polymer layer. An alcohol is introduced into a chamber which is detected by change in the polymer volume, which causes the cantilever to bend [19].

Berger et al. [20] have reported on change in surface stress during the formation of alkanethiol layers in the gas phase on gold coated cantilevers. The surface stress at the monolayer coverage was found to increase linearly with the length of the molecules.

Electrochemical studies have also been carried out by stress measurements with cantilevers [21, 22]. In these studies a metal coated cantilever is placed in a liquid cell. Upon application of a potential between a reference electrode and the metal surface of the

cantilever, a large change in surface stress is produced causing the cantilever to bend due to changes in the electrolyte environment.

The detection of immobilization of single stranded DNA oligonucleotides and hybridization of the complementary oligonucleotide has been demonstrated by Fritz et al. [23] and Wu et al. [24]. In this experiment gold coated cantilever surfaces were functionalized by thiolated probe DNA. Then the target DNA strand is introduced and by measuring the static bending of the cantilever the surface stress change induced by the hybridization was observed.

An example of measuring the change in temperature during a chemical reaction is reported by J. Gimzewski et al. [25].

1.1.2 Dynamic Mode Sensors

There have also been numerous dynamic mode sensors, where not only the stress change but also the mass changes of the cantilever can be measured. The schematic principle of operation can be seen in Figure 1.2. In Figure 1.2(a) the cantilever is vibrating at its resonant frequency, which due to added mass and stress resulting from molecular interactions, gets modified as shown in Figure 1.2(b).

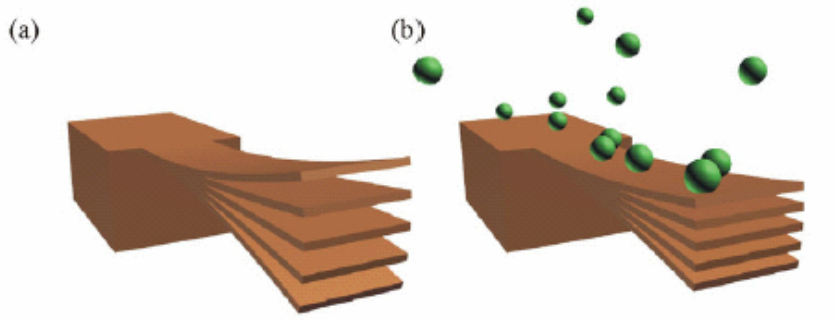

Figure 1.2 (a) Cantilever vibrating at its natural resonant frequency and (b) the resonant frequency shifts due to the added molecular interaction

Through a theoretical treatment of a cantilever based sensor, Sader et al. [26] found that the resonant frequency shift, due to deposition of an evenly distributed mass on the cantilever surface, is induced by a surface stress change as well as a mass increase. Furthermore the two components can be separated.

Baltes et al. [27, 28] have demonstrated high sensitivity alcohol measurements on a cantilever integrated with CMOS circuitry. The cantilever is excited thermally and an integrated piezoresistor reads out the cantilever's vibrational amplitude. A thin polymer layer is deposited on the cantilever and the absorbed alcohol is measured by measuring the resonant frequency shift of the cantilever.

Yang et al. [29] and Cleland et al. [30] have demonstrated the fabrication of nanometer sized resonant structures. The feature size of the mechanical sensor is defined by E-beam lithography. The actuation and detection principle is magnetomotive. The excitation of the device is achieved by passing an AC current through the beam structure and applying a high magnetic field perpendicular to the device, which generates a Lorentz force that drives the beam. The readout is performed by measuring the electromotive force (EMF) across the beam. The deposition of gold has been detected with sensitivity in the attogram range [31].

Several gas sensors have also been demonstrated, where the mass change of a polymer coated cantilever due to chemical gas interaction has been performed [32-35]. Yang et al. [36] have measured hydrogen absorption in carbon nanotubes with ultra thin cantilevers with a thickness down to 20nm. A bundle of nanotubes is attached to the apex of the cantilever and the cantilever is placed in a vacuum chamber. The cantilever is excited by a piezo-actuator and the readout is achieved by a laser doppler system. After

measuring the resonant frequency of the nanotube bundle, the cantilever is placed in a hydrogen gas so that the nanotubes absorb the gas. Then the cantilever is placed back into the vacuum chamber and the resonant frequency is measured again. This system also demonstrated attogram sensitivity [37].

The ultimate mass sensor, based on a nanotube cantilever, has been demonstrated by Wang et al. [38]. In this experiment a TEM is used to observe individual nanotubes in a bundle. An electrode is approached from the top, and the outermost nanotube in the bundle is excited electrostatically and the vibration of the nanotube is observed by the TEM. Then a latex sphere is attached to the apex of the nanotube and the resonant frequency is measured again. With this sensor a mass sensitivity of 10^{-20}g/Hz is reported, which is the best mass sensitivity achieved to date.

1.1.3 Static versus Dynamic Mode

Static mode detection of biochemical species depends on the induction of surface stress changes on the cantilever surface. This means that the interaction of the chemical species must be on only one side of the cantilever in order to maximize the measurable stress signal. This is usually achieved by functionalizing one side of the cantilever so that only one surface is receptive to the wanted biochemical species. The problem of unspecific binding of the wanted or other biochemical species to non-functionalized surfaces is always an issue.

With dynamic mode measurements, both surface stress changes and mass changes of the cantilever can be detected. This means that the desired biochemical species do not have to be connected to one side of the cantilever, but the entire surface area can be used. Thus unspecific binding to the back-side of the cantilever is not a problem.

In dynamic mode both the resonant frequency and the damping of the cantilever can be measured. In this way more information can be accessed by the sensor. Sader et al. and Chon et al. [39, 40] have demonstrated that by measuring the cantilever's resonant frequency and damping effects, the viscosity and density of the gas or fluid around it can be determined, without the need for functionalization of the cantilever. This type of measurement is impossible with static mode detection.

The sensitivity of a static mode biochemical sensor is dependent on the interaction forces between the molecules in a biochemical detector. Typical values of surface stress induced by hybridization of target DNA with the probe DNA are 3×10^{-3}N/m [41]. Hansen et al. have estimated that for probe immobilization, with a probe density of approximately 1013 strands of ssDNA/cm^2, which leads to an approximate sensitivity of 5pg/nm [42] for static mode. Ilic et al. has demonstrated cell detection in air with mass sensitivities of 0.13pg/Hz [43] for the dynamic mode. The main disadvantage of the dynamic mode is that operation in liquids is more complicated and that damping of the cantilever reduces the sensitivity.

1.2 Actuation and Readout Principles for Dynamic Mode Sensors

A schematic diagram of the conventionally used resonant sensor principle is shown in Figure 1.3. The sensor consists of the vibrating mechanical structure and an actuation and detection unit. The actuation unit actuates the mechanical structure into resonance and the readout unit converts the vibration of the sensor into an electrical signal. The signal can then be fed back to the actuation unit in order to maintain peak resonance of the structure.

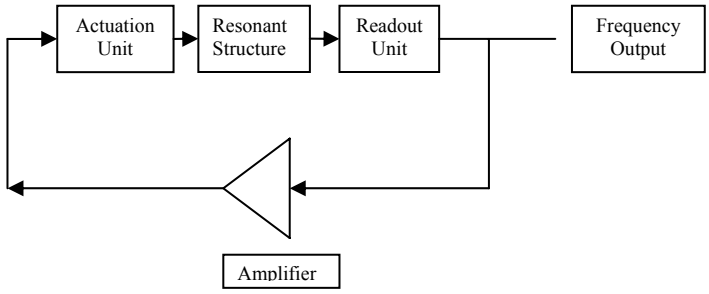

Figure 1.3 Diagram of the resonant sensor principle, which consists of an actuation unit, a vibrating structure and a readout unit

Some of the most common actuation schemes are electrostatic [44], piezoelectric [45, 46], thermal [7, 27, 28, 47], magnetomotive [29, 48] and magnetic [49, 50]. Some of the most common readout schemes are capacitive [44, 51-52], piezoresistive [53-60], and optical detection [16]. However any actuation scheme is bound to add precisely designed electronic components to get the desired overall sensor performance. Also most of the readout techniques have a bulky electronic control. Thus instead of using the traditional design shown in Figure 1.3 and studying the fundamental mode of cantilever vibration, the natural thermal vibrations, associated with the fluctuations in the temperature of the structure, can be used. For a cantilever, the vibrational amplitude is dependent on the square root of the temperature and the square root of the inverse spring constant of the cantilever. Ilic et al. [43] have demonstrated this type of thermal actuation. By scaling down the dimensions of the cantilever, the relative vibration amplitude increases. The challenge is to accurately measure the vibration of the

cantilever, due to the small vibration amplitude. This method can be coupled with the resistive heating, by passing a DC current through a resistor on the cantilever, which increases the temperature and thus the thermal vibration amplitude of the structure.

1.3 Dissertation Summary

In order to have a mass sensor device, the fundamental cantilever vibrational mode has been studied extensively. The cantilever is usually externally excited by different techniques and the shift in the excited frequency is monitored by the techniques mentioned in Section 1.2. The sensitivity associated with this technique can be further enhanced by increasing the resonant frequency and using a small spring constant as discussed with various examples in Section 1.1.2. However, the utility of reducing the cantilever dimension to increase the fundamental frequency can be limited in practice by the difficulty of obtaining reproducible sensitizing coatings on very small surfaces, as well as the need for a suitable deflection detection technique.

As an alternative, recent efforts have begun to investigate the use of higher order flexural modes of cantilever vibration [43, 61-65]. It has been proposed that sensor sensitivity can be improved by using higher order modes for detection because of the associated increase in the frequency of such modes. It has recently been shown [63, 64] that sensor sensitivity using higher order thermal modes should be comparable to reducing the cantilever length. Moreover, Sharos et al. [65] indicate that an increase in quality factor is expected for higher order flexural modes compared to the fundamental mode.

In this dissertation we study the thermally induced fundamental and three higher order modes of Au coated Si cantilevers for Hg sensing. Previously, Hg vapor adsorption

has been demonstrated on Au-coated cantilevers [34, 35, 66-70] using the externally excited fundamental mode of triangular cantilevers. The effects of Hg adsorption on the resonant frequency have been reported for both Au coating along the entire cantilever length and only at the apex. Depending upon the nature of the frequency shifts with Hg exposure, a qualitative analysis of the effect of mass loading and spring constant changes has been proposed [66, 67, 69]. In contrast to these previous studies, we show the possibility of using thermally induced higher order modes of rectangular cantilevers for Hg sensing.

This dissertation is focused on the study of higher order cantilever modes. The optical detection technique is employed throughout this study. The use of thermally induced cantilever modes takes advantage of the possibility of having another in-situ detection technique along with the cantilever deflection without adding to the bulk of the detection system. In this dissertation, I will show how one can use of thermally induced higher order cantilever modes to study both the sensing [82] with cantilever and for studying the basic interfacial interactions during adsorption [85]. Furthermore in an attempt to increase the cantilever sensing response by using a softer cantilever, I will also present experimental validation to the fact that the mode frequency, not the mode order is related to the larger spectral response, is achieved. A new study is carried out where the cantilever thermal spectrum is studied as a function of the percent sensitizing coating area. The analysis of this data may help understand the cantilever's mechanical property changes with variation of sensitizing coating area which opens up good prospects for future work.

1.3.1 Overview of Dissertation

Over the nine chapters in my dissertation, I will present the research I worked on in partial fulfillment of the PhD degree in the Materials Science program.

In the second chapter, I will layout both theoretical and experimental background information pertaining to the study presented in this dissertation.

Chapter Three discusses the design and fabrication of a rectangular silicon cantilever. The fabrication process optimized for different dimensional cantilevers is successfully demonstrated by fabricating straight free standing cantilevers. However these cantilevers are not used for the research presented here mainly because of their thickness tolerance and cost as explained in Section 3.3.

In Chapter Four I demonstrate the use of thermally induced higher order modes for Hg sensing with Au films deposited on a cantilever surface. In Section 3.1 I present the detailed studies which support that the studied modes are the flexural modes of cantilever vibration. In Section 4.3 I give details of a new and simple technique devised to deposit an Au strip of suitable length along one surface of cantilever. The thermally induced modes of the Au coated cantilevers are studied for their sensing response to Hg. It is evident from this study that higher order modes hold promise as another in-situ cantilever detection technique.

In Chapter Five I discuss my efforts to study adsorption interactions at the Au-Hg surface when the sensing Au film is deposited via two different deposition techniques, namely sputter deposition and thermal evaporation. The thermally induced spectral studies of higher order cantilever modes reveal that the surface morphology of the Au film plays an important role in modifying the flexural frequencies of the cantilever

vibrations. A theory based on experimental characterization of these films is presented to explain the differing nature of the frequency response of the two kinds of Au films.

Chapter Six summarizes all the characterization done on the Au films in order to support that the spectral response is primarily due to the Au-Hg interactions. Also the amount and depth of Hg on these films is presented with XPS studies.

Chapter Seven covers the spectral studies as a function of percent Au coverage on a cantilever surface. The changes in the frequency of the first four thermally induced flexural modes are noted when the Au coverage is increased from the free end of the cantilever towards its fixed end. A basic explanation of the spectral behavior is given for this response, however, owing to the novelty of the data, the need for a rigorous analysis is expressed.

In Chapter Eight, I show the design and fabrication of cantilevers made from a polymer (SU-8, a photoepoxy based polymer) material. These cantilevers are studied for Hg sensing under identical conditions to those for silicon cantilevers. This is done in order to check if an increase in the spectral sensing response can be achieved when the cantilever is very flexible. It is proven with experimental evidence from this study that the mode frequency, not the mode order, is responsible for the improved sensing response.

Finally, Chapter Nine is the conclusion to this dissertation. This chapter includes a summary of the research reported in this dissertation, and I present future research avenues in the work covered in Chapters Three to Nine.

1.3.2 New Contributions

Major new work that is presented in this dissertation includes the following:

1. A novel concept of the use of thermally induced higher order cantilever modes to study both the sensing with cantilever and the basic interfacial interactions during adsorption is proposed.
2. The use of thermally induced higher order flexural modes is demonstrated for sensing Hg at the Au coated surface of cantilever.
3. A new yet simple technique to selectively etch Au on one surface of cantilevers has been developed and optimized. Although manual, careful use of this technique can give reasonable repeatability with a tolerance of +/-5μm. The importance of this process is that this process provides access to a relatively unexplored research area of understanding the cantilever property variations with sensitizing coating coverage.
4. The adsorption interactions at the surfaces of Au deposited via two different techniques are investigated.
5. Cantilevers made from the photosensitive epoxy-base polymer, SU-8 have been fabricated and used to check if any improvement in sensing response of the thermally induced higher order modes can be achieved with these low spring constant cantilevers.
6. It is demonstrated for the first time that the full spectral characteristics of the SU-8 polymer cantilevers can be extracted. These cantilevers are further studied for Au-Hg interactions. Although an order of magnitude

increase has been observed for cantilever deflection signal, the spectral response is not improved. So an experimental study to support that the increased sensing response with higher order modes is related to the frequency of the mode and not the mode order is presented.

Chapter 2

BACKGROUND

The theoretical background and motivation of the proposed study is presented in this chapter. The experimental details including the developed experimental setup are given in the second part of this chapter.

2.1 Theoretical Background

The theory related to the thermally induced oscillations of the cantilever will be briefly presented in Section 2.1. It will be further extended to the fundamental mode and the theoretical details about how the externally excited fundamental mode has been employed in sensing will be given in Section 2.2. A review of the thermally induced fundamental and higher order modes is presented in Section 2.3 along with the motivation of the study presented in this dissertation.

2.1.1 Thermally Induced Oscillations

Thermally induced oscillations have been used to study cantilever properties, including the spring constant and Q [71, 72]. The frequency values associated with the flexural modes of vibration can easily be deduced while obtaining the solution to the force equation of cantilever bending in the vertical direction of the beam [73].

Thermal noise, initially from the atomic force microscope (AFM) perspective, has been calculated using the equipartition theorem which states that if a system is in thermal

equilibrium, every independent quadratic term in its total energy has a mean value equal to $\frac{1}{2}k_B T$, where k_B is the Boltzmann constant and T is the absolute temperature. This method takes advantage of the equipartition theorem applied to the potential energy,

$$\left\langle \frac{1}{2} m f_1 z^2 \right\rangle = \frac{1}{2} k_B T ,$$

where f_1 is the resonant frequency, m is the mass and z^2 is the mean square displacement in any mode.

This treatment of thermal noise doesn't directly apply when using the optical deflection detection technique, where the inclination at the end of the microcantilever $\frac{dz(L)}{dx}$ is measured rather than the deflection z itself. Thus to get the thermal noise in the optical deflection detection technique, a proper calibration relation between $\frac{dz(L)}{dx}$ and z can be found.

The following force equation is solved to get the eigenfrequencies of cantilever oscillations.

$$\frac{d^4 \xi(y)}{dy^4} = \alpha_n{}^4 \xi(y) , \tag{2.1}$$

where $$\alpha_n{}^4 = \frac{12 \rho \omega_n{}^2 L^4}{E h^2} . \tag{2.2}$$

ω_n is the angular frequency of the cantilever vibration and ρ is the density of the cantilever material.

Considering the boundary conditions both at the fixed end (x = 0) and at the free end (x = L),

$$\xi(0) = 0, \quad \frac{d\xi(0)}{dx} = 0$$

$$\frac{d^2\xi(L)}{dx^2} = 0, \quad \frac{d^3\xi(L)}{dx^3} = 0 \ .$$

The solution we get is,

$$\xi(y) = A(\cos\alpha_n y - \cosh\alpha_n y) + B(\sin\alpha_n y - \sinh\alpha_n y) \ . \tag{2.3}$$

By solving the above equation for the clamped-free cantilever as shown in Figure 2.1, we get the following transcendental equation,

$$\cos\alpha_n L * \cosh\alpha_n L + 1 = 0 \ . \tag{2.4}$$

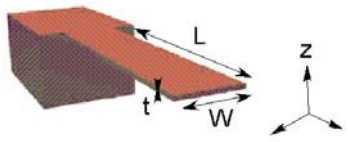

Figure 2.1 A clamped-free cantilever beam

The solution of equation (2.4) gives certain discrete values of α_n which are $\alpha_1 = 1.8751$, $\alpha_2 = 4.6941$, $\alpha_3 = 7.8548$, $\alpha_4 = 10.9955$, $\alpha_5 = 14.1372$ and for other higher order modes, $\alpha_n = \pi\left(n - \frac{1}{2}\right)$.

The values of flexural mode frequencies for a homogeneous, single material, rectangular cantilever, with length L, width w and thickness t, are given by,

$$f_n = \frac{\alpha_n^{\,2}}{4\pi}\frac{t}{L^2}\left(\frac{E}{3\rho}\right)^2 \quad . \tag{2.5}$$

2.1.2 Review of the Externally Excited Fundamental Mode of Vibration

Using equation (2.5), the fundamental resonant frequency of cantilever is given by,

$$f_1 = \frac{1}{2\pi}\sqrt{\frac{\left(\frac{Et^3w}{4L^3}\right)}{\frac{3}{\alpha_1^{\,4}}\rho Lwt}} \quad . \tag{2.6}$$

In its popular form, equation (2.6) can be written as,

$$f_1 = \frac{1}{2\pi}\sqrt{\frac{k}{m^*}} \ , \tag{2.7}$$

where the spring constant, $k = \frac{Et^3w}{4L^3}$, and the effective mass, $m^* = \frac{3}{\alpha_1^{\,4}}\rho Lwt = 0.24m_b$,

with m_b being the mass of the cantilever beam calculated from its density.

In a sensing application with an externally excited cantilever, both the changes in mass and changes in spring constant can change the resonant frequency. The conditions under which the spring constant can change due to adsorption processes involve a change in the surface stress of the cantilever. To account for this, equation (2.7) can be modified as,

$$f_s = \frac{1}{2}\sqrt{\frac{k+\delta k}{m^* + n\delta m}}\ , \tag{2.8}$$

where the initial resonant frequency f_1 changes to f_s due to adsorption. Also, the spring constant k changes to $k+\delta k$ as a result of adsorption induced surface stress while m^* changes to $m^* + n\delta m$ (n , the geometric factor, 0.24 for rectangular cantilevers under study) due to mass loading.

The surface stress on the top and bottom sides of a microcantilever is balanced at equilibrium. Upon differential adsorption on the two surfaces, the unequal stress causes the cantilever to bend. This static bending is usually pronounced and the changes in spring constant and mass change upon adsorption are small. Thus the resonant frequency equation can be approximated, as long as $\delta m^* << m_b$ and $\delta k << k$, by the following equation

$$f_s = f_1\left(1+\frac{1}{2}\left(\frac{\delta k}{k}-\frac{\delta m^*}{m^*}\right)\right)\ . \tag{2.9}$$

Recently many efforts have been carried out to quantitatively decipher between the contributions of δk and δm^* from the final sensor response. The differential surface stress is usually calculated by measuring the deflection of the cantilever upon adsorption and substituting that into the Stoney's relation [74], as follows:

$$\delta s_1 - \delta s_2 \approx \frac{zEt^2}{4L^2(1-\upsilon)}\ , \tag{2.10}$$

where s_1, s_2 are the stresses present on the two surfaces of the cantilever.

The uncertainty related to the Young's modulus of the thin cantilever with respect to the bulk value, mainly in silicon nitrite cantilevers, is taken into consideration and modifications are also proposed [75]. Influence of surface stress on resonance behavior has been studied and a new model has been proposed [76] where the surface stress is monitored by using the shifts observed in the externally excited resonant frequency.

Thus the externally excited fundamental mode has been largely studied from all perspectives of sensing with cantilevers. There have been many efforts to improve the detection sensitivity of fundamental modal frequency [36, 37, 77, 78]. Two main solutions sought for this purpose are taken from the scaling law. Assuming pure mass loading, the change in mass of the microcantilever after adsorption can be found as,

$$\delta m = \frac{k}{4\pi^2}\left(\frac{1}{f_s^{\,2}} - \frac{1}{f_1^{\,2}}\right) . \tag{2.11}$$

If the mass change is sufficiently small, the frequency change can be approximated as follows:

$$\frac{\delta f}{\delta m} \approx \frac{2\pi^2 f_1^{\,3}}{k} . \tag{2.12}$$

Thus, the scaling law, equation (2.12), suggests a large resonant frequency and a small spring constant, i.e., a smaller and thinner cantilever, can lead to a more sensitive response. Many efforts have been done to reduce the cantilever dimensions, and using the resultant higher fundamental modal frequency, sensitivity in the attogram regime has been achieved [37, 77, 78]. However, the utility of reducing the microcantilever dimension to increase the fundamental frequency can be limited in practice by the

difficulty of obtaining reproducible sensitizing coatings on very small surfaces, as well as the need for a suitable deflection detection technique.

Although highly sensitive detection is possible with the externally excited fundamental mode's spectral response, it is important to note that this technique needs external circuit elements adding to the bulk of the optical deflection detection system. The spectral measurement with other detection mechanisms such as piezoresistive or capacitive is also highly dominated by the associated electronics.

2.1.3 Proposed Study: Thermally Induced Higher Order Modes

In the search for an in-situ detection scheme to alternately detect the sensing response of the cantilever, studies of thermally induced higher order modes have been proposed. The beauty of studying all observed higher order flexural modes simultaneously and at ambient conditions, without the need for any additional circuit elements or external signal sources is what persuaded me to take on this research. Although recent studies show an aggressive trend towards solving the δk and δm^* contributions from the sensor response, it is believed that the detailed study of the thermally induced higher order modes with respect to the sensitizing coating coverage, would lead to major clues in this puzzle, and that is another reason this study would prove to be helpful. Although this approach looks promising, the main problem that is foreseen is the low Qs associated with the thermally induced modes. Thus to improve the sensitivity of detection, as suggested by equation (2.12), use of lower Young's modulus material to lower the cantilever spring constant is proposed as the cantilever material. Polymers are considered ideal for this purpose because of their low Young's moduli, ease of fabrication and relative inexpensiveness.

In this section, the review of the use of thermally induced fundamental and higher order modes is presented.

Thermally Induced Fundamental Mode

The thermally induced fundamental mode has mainly been studied to determine the spring constant of the cantilever [71, 72]. Measuring the frequency before and after adding a known mass at the end of the cantilever, the spring constant has been deduced. This non destructive technique proved the necessity of calibrating the cantilevers for force sensitive measurements. The scaling of the spring constant with the cube of the unloaded frequency has been demonstrated in these studies.

The thermally induced fundamental mode has also been employed to estimate the mass of the functional layer on the cantilever [31, 79]. As mentioned earlier, one surface of the cantilever is usually functionalized for its use as sensor. The frequency shifts observed before and after the coating of the functional layer have been used to calculate the mass of that layer. This method works well when the added mass is mainly located at the end of the cantilever beam, so that the δk changes do not interfere with the mass calculation. However this technique is used for cantilevers with a functional layer along the entire length.

Thermally Induced Higher Order Modes

Initially from the AFM imaging perspective, the thermal noise was considered interference in obtaining optimum images [72]. There is a wide variety of literature

pertaining to the theories of the thermal noise in the mid 1990s [73]. Many of those papers are oriented towards finding the relation between the amplitude of the thermal vibrations and the cantilever properties such as spring constant to the ambient temperature.

Recent efforts show a trend towards the study of thermally induced higher order modes rather than applicability perspectives [61-65]. Schaffer et al. [61] has studied the flexural vibration modes of a cantilever with an optical detection technique suggesting the advantages of the use of higher order modes for imaging and spectroscopy applications. Models close to the actual sensing scenario have been proposed to accommodate for real time situations and to incorporate the real factors affecting the higher order modes into the analytical theory. For example, the modification to the basic thermal oscillation theory presented in Section 2.1, where the effect of the addition of the functional layer onto the thermal flexural spectrum has been taken into account, has been presented [62]. The analytical solution then becomes,

$$f_n = \frac{{\alpha_n}^2}{2\pi L^2}\left(\frac{\int_h E(z-z_0)^2\,dz}{\sum_i^n t_i\rho_i}\right)^{\frac{1}{2}} . \qquad (2.13)$$

The analytical solution of a multilayered cantilever has been validated by comparing the solution with the values obtained from finite element simulation [62].

With the comparison between using higher order modes and reducing cantilever dimensions, F. Lochon has shown that sensor sensitivity using another higher order

modes is as good as reducing cantilever length [63]. Thus, a simple yet promising use of the higher order modes has been suggested for sensing applications.

Thus with this review, it can be stated that the recent literature implicitly supports the promise the higher order thermal modes hold in different applications. However, it's worth noting here that sensing with thermally induced higher order modes has not been demonstrated in the literature.

2.2 Experimental Details

The optical deflection technique where a laser beam is focused at the tip of a rectangular cantilever and the motion of the reflected spot is monitored on a position sensitive detector (PSD), is used throughout the studies presented in this dissertation. A commercial atomic force microscope (AFM) head purchased from Digital Instruments is used where cantilevers are mounted in a commercial (Digital Instruments) glass holder. A gas flow setup and Hg delivery setup is designed and built in order to carry out the experiments. The associated electronics to extract the AC component of the PSD signal and amplify it has been developed by Dr. Asit Kar [81] and is used without further modifications throughout this study. The cantilever deflection signal is also monitored during all the studies presented here, so the efforts to get steady drift baseline are also presented in this section. Also reasons for the choice of the Au-Hg sensing system are given in the last section.

2.2.1 Experimental Setup

The experimental setup used for this study is shown in Figure 2.2. The laser reflection technique is employed to measure both the cantilever deflection and resonance spectrum. Teflon gas tubing and Aalborg mass flow controllers are used to deliver either

N_2 or analyte gas to the gas chamber where the cantilever is held. An Au-coated cantilever is placed in a gas chamber with constant N_2 flow and exposed to pulses of Hg vapor. A Hg effusion tube (Vici Scientific), placed inside a Dynacalibrator (Model 190, Valco Instruments Co. Inc.) at 40^{o}C, with 32.576ng/min effusion rate is used to precisely control the Hg concentration, which is constantly monitored at the exit of the gas chamber with a Jerome 431-X Hg vapor analyzer (Arizona Instruments, Phoenix, AZ). A commercial Hg trap is used to collect any Hg at the Valve 1 or after the Hg detector.

The deflection of the cantilever is recorded with a computer controlled data acquisition system and the thermal spectral response is recorded using an HP3588A Spectrum Analyzer.

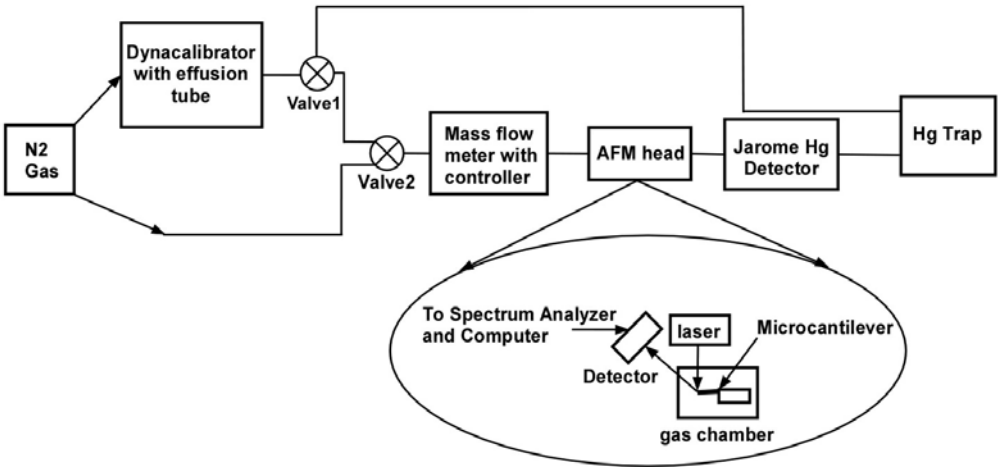

Figure 2.2 Experimental Setup. Valve 2 is a 3-way valve which connects the gas chamber either to nitrogen gas or mercury vapor depending upon its position

2.2.2 Deflection Drift Stabilization

Many different factors including, but not limited to, laser heating, environmental instability environmental noise, etc., cause drift in the deflection signal. Containing the cantilever in the gas chamber with constant flow of dry N_2 was used to avoid environmental noise effects. Clean, flushed Teflon tubing, non-contaminated dynacalibrator, etc., have been maintained and after the initial 20-40 minutes drift time, as seen in Figure 2.3, the deflection drift usually becomes stable.

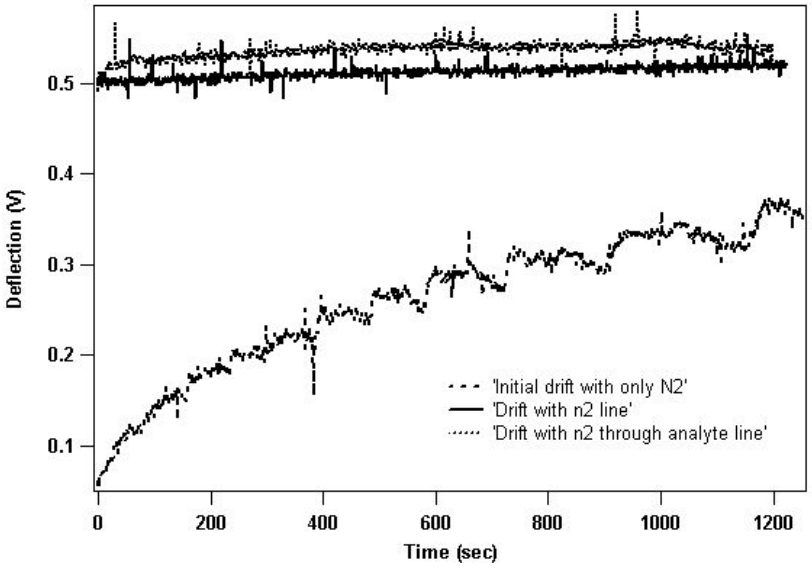

Figure 2.3 Stable deflection baselines are observed after an initial drift stabilization period of 20-40 minutes

The effects of many parameters such as ambient temperature fluctuations, gas flow fluctuations, switching of valves 1 and 2 (Figure 2.2) are thoroughly studied in order to understand the baseline for deflection measurements. Two examples are presented here.

Example 1. To study the effect of ambient gas temperature variation at the cantilever, the temperature at the gas chamber is monitored as the dynacalibrator temperature was ramped to 85^{o}C from RT. The cantilever deflection drift observed with N_2 flowing through the dynacalibrator and N_2 flowing through the other path (Figure 2.2 with valve 2 closed so that N_2 flows via Dynacalibrator to the Hg trap) is monitored. Figure 2.4 shows the temperature increase at both, the dynacalibrator and the gas chamber. Usually a temperature rise of 0.4^{o}C is observed at the gas chamber with the dynacalibrator heating from room temperature to 85^{o}C.

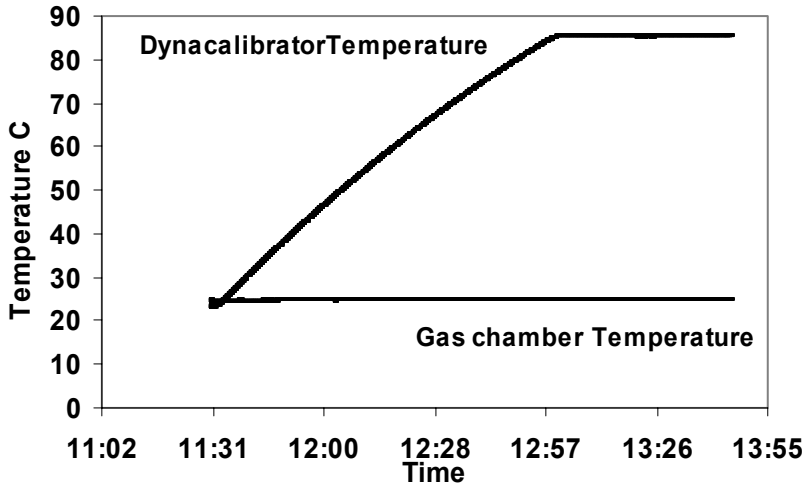

Figure 2.4 Dynacalibrator chamber temperature and gas chamber temperature as a function of time

The related drift is shown in Figure 2.5. The dotted line shows the stable drift with N_2 flowing through the nitrogen line and the solid line shows the N_2 flowing through the analyte line. Although there is a small change in the magnitude of the drift, it is still acceptable for our experiments.

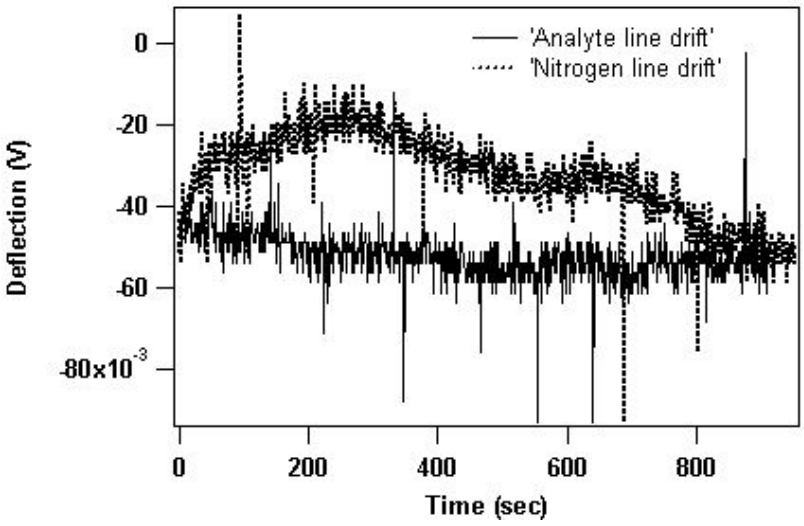

Figure 2.5 Deflection drift with the variation of temperature

Example 2. The effect of flow variations on the drift has been studied by changing the N_2 flow rate from 75sccm to 100sccm with time as seen in Figure 2.6. The drift observed in the baseline is found to be +/-20mV and was acceptable.

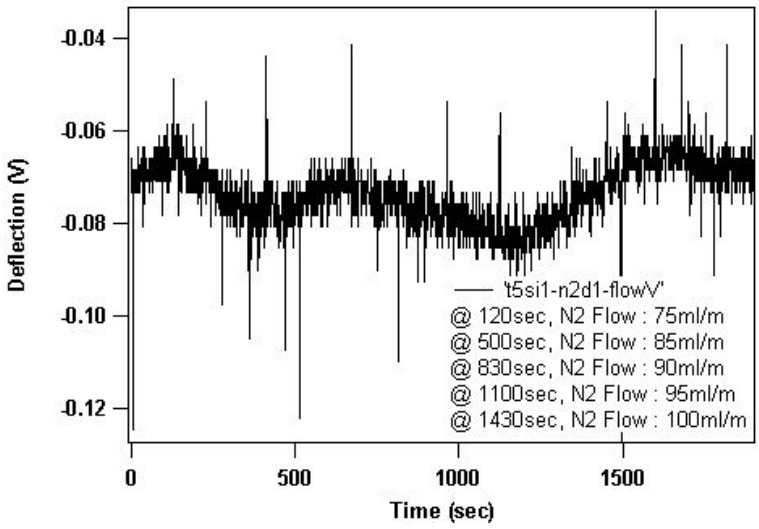

Figure 2.6 Deflection drift with the variation of N_2 gas flow

2.2.3 Choice of Sensing System

Although there are a diverse variety of chemical, biological and physical sensing systems studied with the cantilever, the Au-Hg system was selected for the proposed study. The dominating reason associated with this choice was having Au as the sensing element, mainly because of the ease and reproducibility of the deposition on one surface of the cantilever. Also, if needed, various deposition techniques including sputtering, thermal evaporation or e-beam evaporation were readily available to study an optimum Au surface morphology for the Hg adsorption study. As discussed in Chapter Four, because of the simple wet etching technique available for the Au surface, the repeatable deposition (tolerance: +/-5μm) of end loaded cantilevers became possible. Another reason for this choice was the possibility of developing a relatively inexpensive yet very precise Hg delivery system as described in Section 2.2.1.

2.3 Conclusions

In this chapter, the theoretical concepts and experimental tools behind the work presented in this dissertation are introduced. The basic ideas related to the conventional approach using an externally excited fundamental mode and its theoretical extension to the thermally induced higher order modes, which is necessary to understand the work in this dissertation, are introduced. The advantages of the proposed study are outlined, which in turn supports the motivation of this work. The drawback of the low quality factors due to the small vibration amplitudes associated with the proposed technique are outlined along with one solution to overcome those. The summaries of the experimental setup and baselines optimized and employed in this dissertation follow at the end.

Chapter 3

SILICON MICROCANTILEVER FABRICATION

This chapter covers the microfabrication process optimized for silicon cantilevers. Although originally it was proposed to use such fabricated cantilevers in my studies, they were not used mainly because of the cantilever thickness tolerance and their cost. However the in-house fabrication of Silicon cantilevers has been demonstrated by fabricating different dimensional cantilevers with 66% yield per wafer. This chapter documents the fabrication process and its results.

3.1 Introduction

Silicon cantilevers have been used extensively for both sensor research and Atomic Force Microscopy (AFM) applications. A number of commercial vendors provide the cantilevers needed for all the conventional AFM applications. These and other vendors also supply the cantilever research community with custom made, application suitable cantilevers. However, getting a suitable cantilever custom made from these vendors is often limited by associated cost and minimum required purchase.

With the availability of a state of art microfabricaton facility at the Nano-Micro Devices Center (NMDC) at UAH, we decided to microfabricate rectangular, free standing cantilevers for our research. The details of the fabrication are presented in Section 3.2.

3.2 Silicon Microcantilever Fabrication

The cantilever material was chosen to be Si mainly because of its wide use in sensor research at UAH. Also the optimized process for Si cantilever fabrication can be applied towards other cantilever materials such as silicon nitrite. The second important choice to be made for the microfabrication process was whether to release cantilevers from the wafer by wet or dry chemical etching. Since wet etching involved developing a separate wet bench with rather daunting specifications due to the toxicity levels involved, it was decided to use a dry etching technique for release. Because of the unavailability of the licensed deep etch (Bosche) process at UAH, it was decided to use the process available at Auburn University.

3.2.1 Fabrication Process

A Silicon on Insulator (SOI) wafer with the desired device layer thickness (2μm) and buried oxide (BOX) layer thickness (750nm) is used as the substrate. The detailed cantilever fabrication process is shown in Figure 3.1, which can be broadly divided into the following five steps.

1. Transfer of alignment marks on both sides of SOI wafer
2. Cantilever definition
3. Delay and deep mask definition
4. Delay and deep etch
5. Wafer Release

Each of these steps is explained briefly.

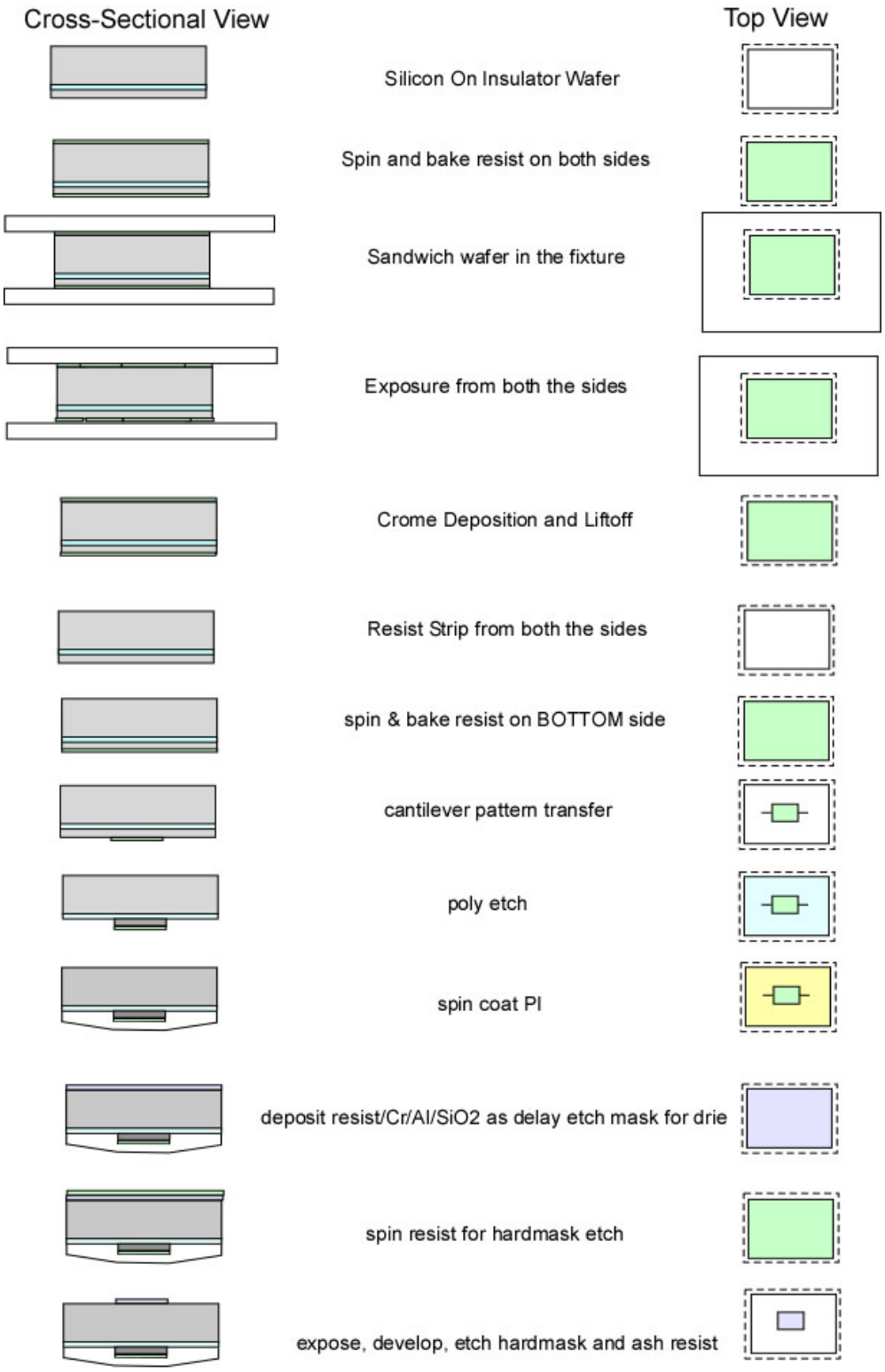

Fig. 3.1 Detailed Si cantilever fabrication process

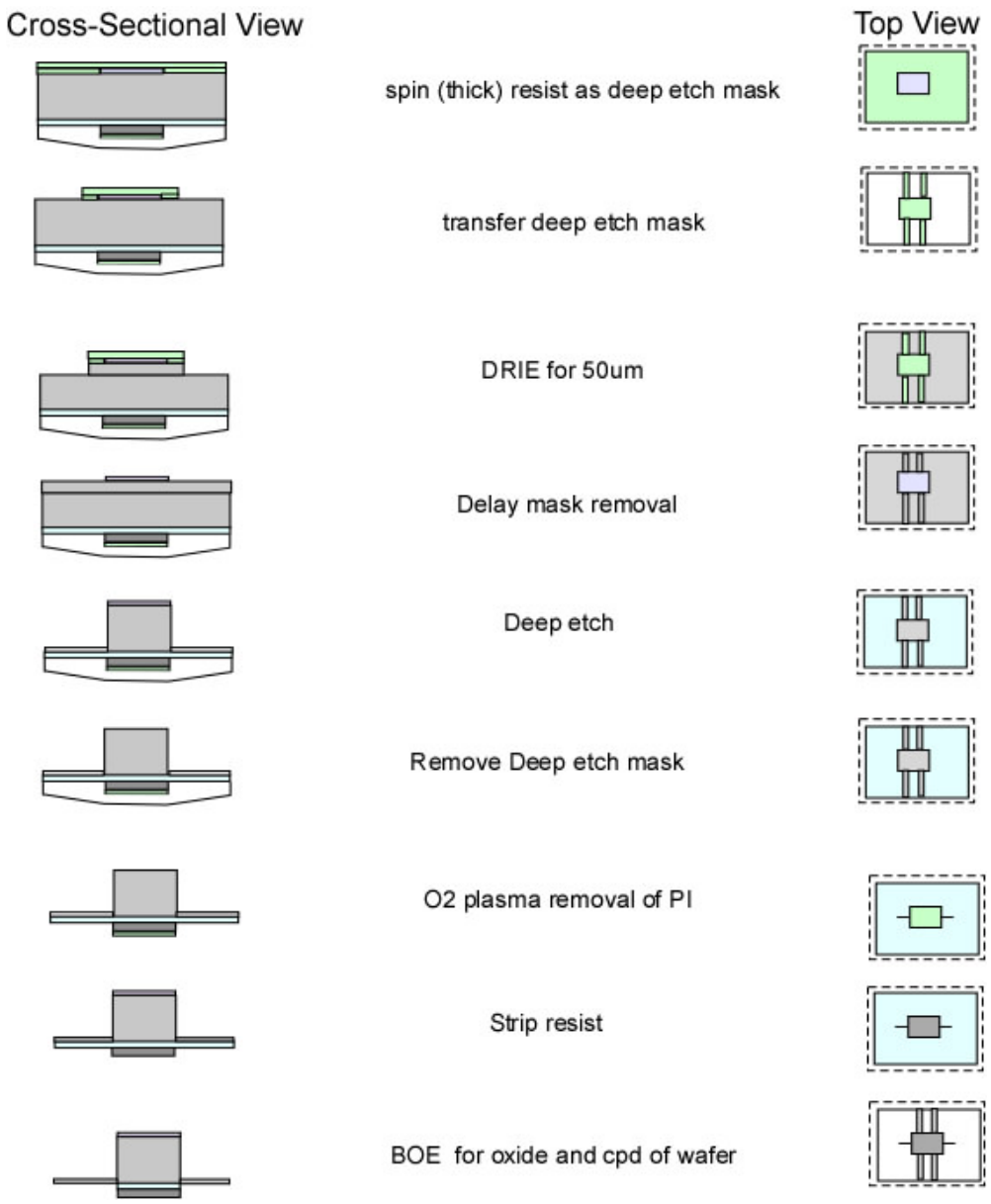

Fig. 3.1 Detailed Si cantilever fabrication process, continued

Fabrication Step 1. Transfer of Alignment Marks on Both Sides of SOI Wafer

Since we chose the dry deep etch process, the fabrication involved processing the SOI wafers from both the sides while maintaining good alignment accuracy between the

bottom surface (the device side of the SOI wafer where cantilevers are defined) and the top surface (the SOI surface where the deep and delay etches are carried out). In order to facilitate the dual surface micromachining, the top and bottom alignment marks must be aligned to each other as well as the subsequent photolithography layers.

(a)

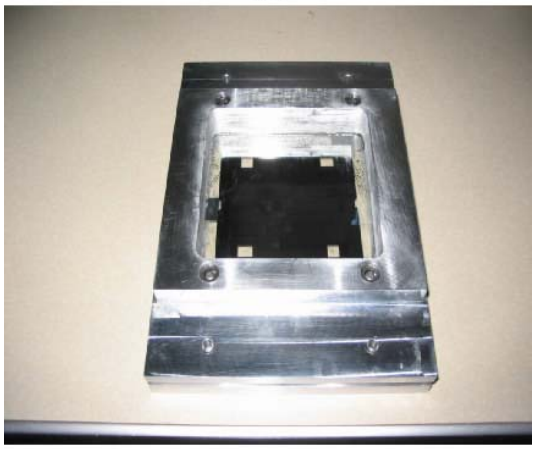

(b)

Fig. 3.2 Two sided alignment fixture. (a) Top (left) and bottom (right) alignment plates with respective alignment masks attached to them and (b) The fixture after alignment, the SOI wafer is sandwiched between the two plates

To do this, a double sided alignment fixture is designed having two Al plates which can be accurately placed and fixed on top of each other as shown in Figure 3.2.

The top and bottom photolithographic masks, each with two sets of alignment marks are aligned and attached to the top and bottom plates of the fixture respectively. This is done with the help of the four corner alignment windows on the two masks (Figure 3.2(a)). This alignment is done by placing the fixture on a specially made optical microscope stand with the help of an 'Olympus BX60' optical microscope. The best alignment between the two masks is observed to be within a tolerance of +/-10μm.

The SOI wafer is placed (top side up, device layer facing down) on top of the bottom alignment mask and is aligned to that mask with the help of some alignment features placed on the mask. The top fixture plate having the attached mask is then lowered on top of the bottom fixture plate having both the bottom alignment mask and the SOI wafer. Then the top fixture plate is fitted to the Thompson rods of the bottom fixture plate. Once the four corner thumb screws are fitted at the corners of the double sided alignment fixture, the first photolithography process is carried out and the two sets of active alignment marks are transferred on each side of the SOI wafer. The use of this fixture gives alignment accuracy of +/-10μm between the top and bottom surfaces of the SOI wafer.

Fabrication Step 2. Cantilever Definition

This step consists of cantilever definition, dry Si etch and bottom surface protection. The photolithographic step involves transferring the cantilevers on the bottom side of the SOI wafer. This is done by UV exposing the photoresist coated bottom side with a photolithographic mask having cantilever structures and developing it. The cantilevers are defined by a SF_6 based RIE etch of Si with photoresist as the etch mask. After this step, the other side, that is the top side of the SOI wafer, needs to be processed,

so to avoid any damage to the defined cantilever structure on the delicate device layer, this side is protected with polyimide (PI 2661, Microchem Co.) coating. Once protected with Polyimide, the bottom surface of the wafer is attached to a handle wafer with a metallic paste (Cool Grease, Angstorm Sci.) to maintain good thermal contact necessary during the deep etch.

Fabrication Step 3. Delay and Deep Mask Definition

To facilitate easy handing of the cantilever dies once the whole wafer is released, thin Si tabs extending laterally from the die to the wafer grid are used. This is carried out as a delay etch of the tab features before carrying out the deep etch. The hard mask (SiO_2) is first deposited on the top SOI side. Then the top SOI surface is aligned and patterned with the delay etch mask which has tabs between the die and the wafer grid. 500nm sputtered SiO_2 is used as the hard mask for etching the patterned delay tabs on the topside of the wafer. A thick negative photoresist (STR 1075, Microchem Corp.) is used as the deep etch mask. The top SOI side is then spun and patterned with the deep etch mask. The thickness of this mask layer is 8μm.

Fabrication Step 4. Delay and Deep Etch

The wafer is then transported to Auburn and the first Si etch for the delay tabs is carried out for an approximate thickness of 50μm with the SiO_2 mask. The SiO_2 is then etched in buffered oxide solution, and the wafer is further etched all the way through with the thick photoresist etch mask. The wafer becomes very fragile at this point because approximately 50% of the SOI wafer is etched during the dry etch. The wafers are transported then to Huntsville with the handle wafer still attached.

Fabrication Step 5. Release

The handle wafer is removed from the SOI wafer with an overnight acetone soak. The buried oxide from the SOI wafer is wet etched in a buffered oxide solution. Lastly the cantilevers are released after ashing the polyimide in the Reactive Ion Etcher (RIE) with oxygen.

3.2.2 Mask Making

There are a total of five photolithographic masks as mentioned below used in this microfabrication process.

1. Bottom Alignment Transfer Mask
2. Top Alignment Transfer Mask
3. Cantilever Definition Mask
4. Delay Etch Mask
5. Deep Etch Mask

All but the cantilever definition mask are made with mylar plots and crome on Soda lime glass plates. The process for making these masks involves designing the masks using either LEdit or LASI CAD software, ordering the mylar plots for the designed mask layers and transferring the mylar patterns onto the soda lime glass with anti reflective crome coating. Thus it's a very low cost process with the downside of least alignment accuracy (+/-10μm) and more edge roughness of the mask features (500nm). Having good edge roughness is critically important for the cantilever definition mask, so that mask was not made in house but was ordered from Compugraphics USA. The rest of the masks were designed in such way that a total misalignment of 25μm was tolerated by the features.

3.2.3 Fabrication Optimization

The following parameters were needed to be optimized before straight free standing cantilevers could be fabricated.

1. Very careful use of the double sided alignment fixture is important for the successful cantilever fabrication. During the exposure of the two sides of the SOI wafer, the fixture needs to be flipped, and careful handling can avoid more misalignment at that point.
2. Rounding at the corner of the cantilever dies as a result of large misalignment was significant. To correct for this a new set of delay and deep etch masks was designed where the die size was increased by 25µm laterally in comparison to the die size on the cantilever definition mask. This provided additional tolerance to the misalignment, and the rounding of the die at the edges was not seen.

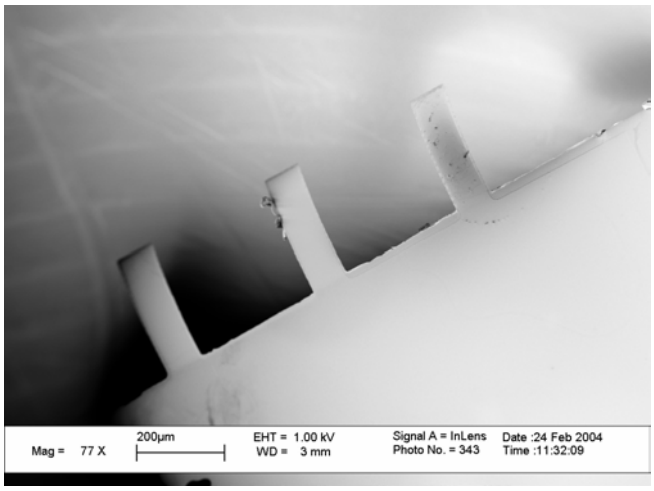

Figure 3.3 Bent cantilevers

3. The polyimide used to protect the bottom side of the wafer after the cantilever definition was removed as the last step in the cantilever. The ashing recipe needed rigorous optimization because any etch non uniformity over the 4" wafer area resulted in bent cantilevers.

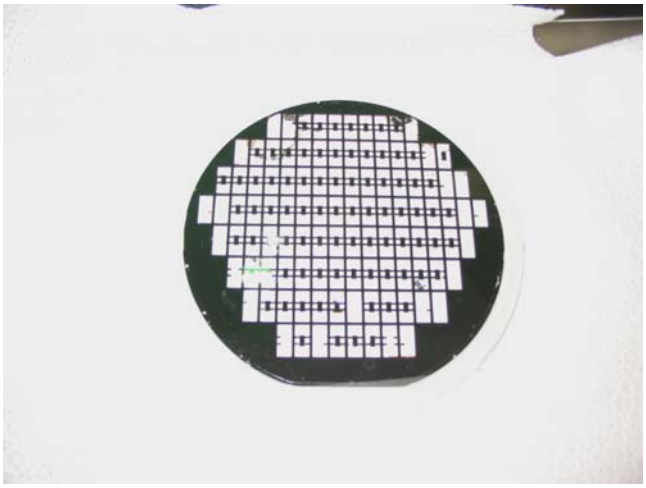

(a)

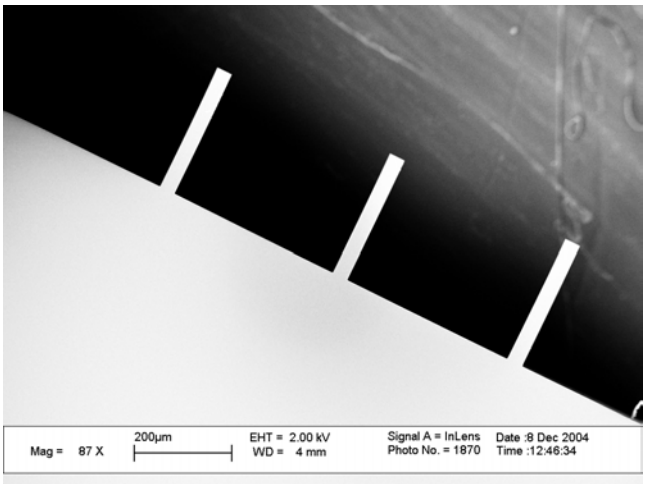

(b)

Figure 3.4 (a) A fully released SOI wafer and (b) Scanning electron microscope image of straight free standing cantilevers

4. Even after optimizing all the above, the cantilevers mostly were found to be bent as seen in Figure 3.3. This was attributed to the stress at the base of the cantilever. In order to compensate this stress and keep it from bending the cantilevers, the cantilever definition mask was redesigned where instead of cantilevers hanging right at the very base, they were extended back by 10μm on the cantilever die. The free standing length of the cantilever was not altered by doing this. As a result straight cantilevers were fabricated as shown in Figure 3.4.

3.3 Conclusions

The Si cantilever fabrication process has been successfully demonstrated where SOI wafers were used as substrates along with the dry chemical etch process for deep etching Si. Free standing straight rectangular cantilevers with different dimensions have been fabricated. A 66% yield per wafer has been observed, which is low mainly due to the non uniformity of the deep etch across the 4" wafer. This fabrication process can be applied with some modifications to other hard cantilever material such as Silicon Nitrite. It is found that 50% thickness variation was associated with the SOI wafer from the batch, which was considered undesirable for our spectral studies. Also the cost of the SOI wafers as compared to commercially available custom Si cantilevers and unavailability of the licensed deep etch process at UAH were other factors for not using the fabricated cantilevers for further studies.

Chapter 4

USE OF THERMALLY INDUCED HIGHER ORDER MODES OF A MICROCANTILEVER FOR MERCURY VAPOR DETECTION

In this chapter the demonstration of the use of thermally induced higher order cantilever modes for mercury detection is presented [82]. The details of the study of the first four thermally induced flexural modes (i.e., the fundamental and first three higher order modes) of rectangular Si cantilevers examined for two different Au coatings are given. In the first case, 50nm thick Au is sputter deposited along the entire length of a rectangular Si cantilever (called hereafter a 'Fully Loaded Cantilever'). In the second case the Au is confined to a 30μm length at the tip of the Si cantilever (called hereafter a 'End Loaded Cantilever'). In both cases the cantilever spectral response and deflection has been studied as a function of Hg concentration and total exposure time. For the low doses studied, the higher order modes show a distinct Hg sensing response whereas the fundamental mode does not.

4.1 Microcantilever Thermal Spectrum

A typical thermal resonance spectrum of a cantilever is shown in Figure 4.1, where the amplitude of vibration in units of dBm is plotted on the y axis. The inset shows the analytically calculated equivalent root mean square amplitude in nm. Note that four distinct modes are readily discernable.

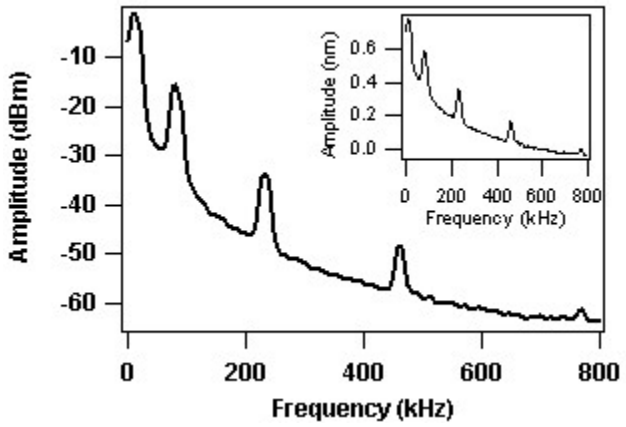

Figure 4.1 A typical thermal resonance spectrum of a microcantilever

The measured modal frequencies are shown in the last column of Table 4.1. These have been verified to be flexural modes by comparison with the results of three different techniques as shown in Table 4.1. Analytical calculations based on References 61 and 62 that take into account the effect of the Au coating [83] are used to theoretically determine the frequencies and are shown in column 2 of Table 4.1.

Table 4.1 Comparison of the values of modal frequencies obtained by different techniques

Mode	**Theoretically Calculated Frequency(Hz)**	**FEM Frequency(Hz)**	**Frequency measured with active excitation with D3000 AFM (Hz)**	**Experimentally measured Frequency(Hz) (Observed Standard Deviation Hz)**
1	12,832	12,786	12,780	12,766 (0.913)
2	80,422	80,127	78,870	78,991 (2.754)
3	225,185	224,345	225,660	225,990 (5)
4	441,273	439,585	446,160	446,460 (7.071)

The third column has resonance frequencies calculated by finite element analysis. In addition, a Digital Instrument Dimension 3000 AFM is used to actively excite the cantilevers and measure the frequencies. These are shown in the fourth column. Note that

the experimental values for the thermally excited modes match very well with the results obtained from the other techniques.

The experimentally calculated quality factors for the four measured modes are shown in the first row of Table 4.2. It can be seen that the quality factor increases approximately by a factor of 10 when the 2nd order mode is used instead of the 1st order mode. The quality factor increases by a further factor of 3 when the 3rd order mode is used instead of the 2nd order mode. Similarly in going from the 3rd order mode to the 4th order mode, an approximate increase by a factor of 2 is seen.

Table 4.2 Comparison of experimentally observed and theoretical [63, 64] quality factors

Mode Order, N	**1**	**2**	**3**	**4**
Experimental quality factor	1.475	11.177	33.078	67.770
Experimental quality factor Increase $\frac{Q_N}{Q_{N-1}}$	-	7.6	3.0	2.1
Calculated Support Loss [Ref. 63]	$5.7*10^6$	$4.7*10^5$	$1.7*10^5$	$8.9*10^4$
Theoretically calculated increase in Q_{sup} $\frac{Q_N}{Q_{N-1}}$	-	12.1	2.8	2.0

As suggested in References 63 and 64, the support loss is significantly different for higher order modes compared to the fundamental mode of cantilever vibration. Support loss, also known as clamping loss, is the vibration energy of a resonator

dissipated by transmission through its support. The quality factor associated with support loss, Q_{sup}, as calculated by Equation 22 of Reference 63 is shown in Row 3 of Table 4.2 for the cantilevers used in this study. Note that Q_{sup} increases by approximately a factor of 10, 3 and 2 when going from 1st to 2nd, 2nd to 3rd, and 3rd to 4th order modes respectively, which is comparable to what we observe for the measured quality factors. Thus the limitation on the increase in the quality factor of higher order modes appears to be primarily associated with the support loss.

4.2 Fully Loaded Microcantilever

To fully load bare Si cantilevers with Au, 5nm Cr and 50nm Au is sputtered on the top surface. The cantilever is then placed in a gas chamber where the N_2 gas flow is maintained at 90sccm and the spectral response is recorded.

After deflection drift stabilization, a cantilever is exposed to a 15ppb concentration of Hg for 100sec. The spectral data is recorded 1000sec after the Hg exposure has been stopped. This gives enough time for the deflection signal to stabilize as shown in Figure 4.2(a). Four more subsequent exposures of Hg are then carried out under identical conditions and the spectral data is taken after each exposure. No saturation in the deflection response of the cantilever is seen for subsequent Hg exposures. However, the deflection amplitude decreases slightly with increasing number of exposures. For example, by comparing the cantilever's deflection amplitude after the first and fifth exposure, an approximately 20nm decrease in deflection is observed for the last exposure compared with the first. Figure 4.2(b) shows the frequency shifts (i.e., mode frequency prior to Hg exposure minus the mode frequency after the Hg exposure) of the first four flexural modes of the cantilever as a function of total Hg exposure time.

The 4th order mode undergoes a frequency shift of -360Hz whereas the first order mode shows almost no shift for a total exposure time of 500sec. Note that the frequency shifts of the higher order modes essentially saturate after the 4th Hg exposure.

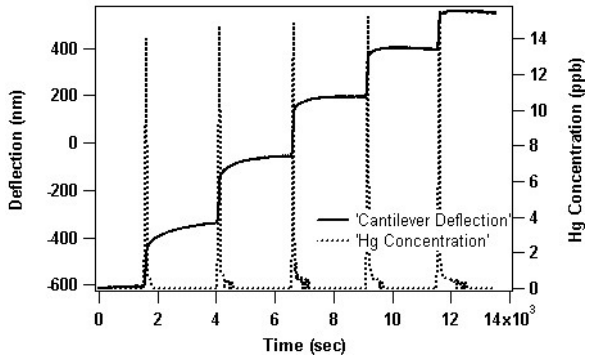

(a)

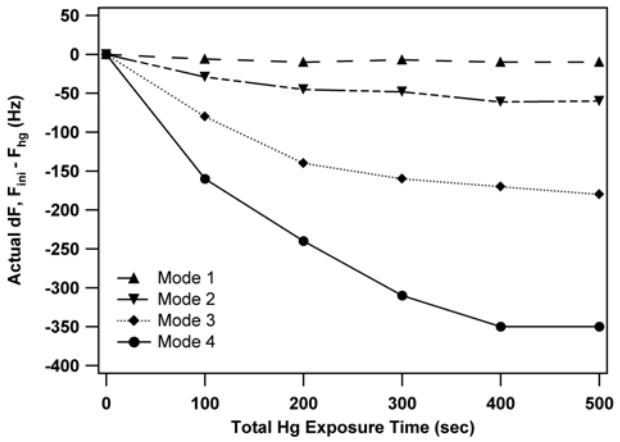

(b)

Figure 4.2 (a) Deflection of a fully loaded microcantilever as a function of Hg exposure time. (b) Spectral response of a fully loaded microcantilever as a function of total Hg exposure time (difference between the microcantilever's modal frequency before and after Hg exposure).

The observed frequency shifts for the higher order thermally induced modes are negative for fully loaded rectangular cantilevers in which the Au layer is sputtered. The fundamental mode shows a shift of only -3Hz. In the literature [66, 67], the externally excited fundamental mode of a fully loaded triangular cantilever having thermally evaporated Au as the Hg sensing surface shows positive frequency shifts, which is opposite to what we report here for higher order modes. Initial experimental results in our laboratory for thermally evaporated versus sputtered Au films indicate that the difference in sign is related to the interfacial energies associated with the surface morphology of the Au coating, which is different for the two deposition methods.

4.3 End Loaded Microcantilever

We turn now to an examination of frequency shifts for higher order thermal modes upon Hg adsorption for end-loaded rectangular cantilevers. To fabricate end-loaded cantilevers, use of shadow masks has been proposed [84]. Here we employ a simple new technique, in which the Au is selectively wet etched with photoresist as an etch mask. Figure 4.3 shows optical microscope pictures at various stages in the end-loading process. A bare Si cantilever is first sputter-deposited with 5nm Cr and 50nm Au. A borosilicate glass micropipette with 10μm inner diameter is used to dispense a known amount of photoresist onto the tip of the cantilever. The amount dispensed via micropipette is controlled by a nanoliter injector (Nanoliter-2000, World Precision Instruments). The photoresist is then soft baked at 90^{o}C for 2 minutes. The Au is wet etched for 2 minutes in Au etchant (GE-8110, Transene Company, Inc.) The photoresist etch mask is stripped in acetone for 5minutes. The cantilever is then subjected to oxygen

plasma (100W, 100mT, 40sccm O_2 in a PlasmaTherm System 790) for 5 minutes to remove any residual photoresist.

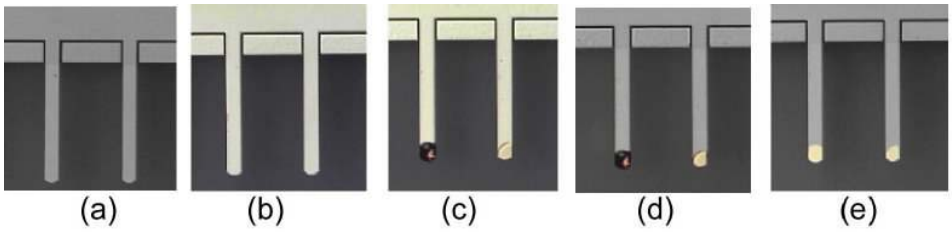

Figure 4.3 Process of end-loading the microcantilever (a) bare Si microcantilever, (b) 5nm Cr, 50nm Au coated microcantilever, (c) tip-coating of photoresist (the contrast between the two photoresist coatings at the tip indicate two different dispensed volumes), (d) after Au etch with photoresist as the etch mask and (e) End-loaded microcantilevers after photoresist strip and oxygen descum. The Au area is 1015μm^2.

After measuring the thermal resonance spectrum prior to Hg exposure, an end-loaded cantilever is exposed to a 14.5ppb concentration of Hg for 100sec. The deflection is continuously monitored [Figure 4.4(a)] and the spectral data is recorded 1000sec after the Hg exposure. Two more identical 100sec exposures are carried out. In Figure 4.4(b) the frequency shifts of the first four flexural modes of the cantilever are shown as a function of the total Hg exposure time. As seen in Figure 4.4(b), after a continuous decrease in the 4^{th} order modal frequency, a sudden increase by 20Hz after the third Hg exposure is observed. To check out this discrepancy and to find the nature of the frequency response, two higher concentration exposures (20 ppb), i.e., the fourth and fifth exposures in Figure 4.4(a), for a longer time (300sec) were performed.

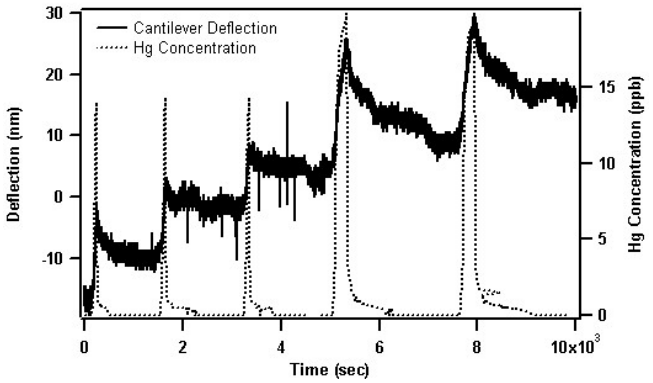

(a)

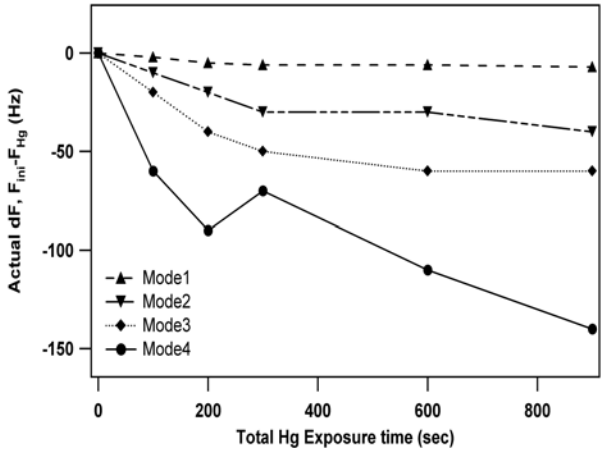

(b)

Figure 4.4 (a) Deflection of an end loaded microcantilever as a function of Hg exposure time. (b) Spectral response of a fully loaded microcantilever as a function of total Hg exposure time (difference between the microcantilever's modal frequency before and after Hg exposure)

Note that in contrast to the deflection response of the fully loaded cantilevers, the deflection signal in Figure 4.4(a) decreases after the fourth and fifth exposures. This may indicate that some Hg desorbs from the cantilever. Also note that the spectral shifts of the 2^{nd} and 3^{rd} order modes almost saturate after the 4^{th} exposure. For a total exposure time

of 900sec, the 4^{th} order mode undergoes a frequency shift of –140Hz whereas the first order mode shows almost no frequency shift, similar to the fully loaded cantilever case.

4.4 Conclusions

In this chapter, the use of thermally induced fundamental and first three higher order modes of rectangular cantilevers for Hg sensing is demonstrated. These modes are verified to be the flexural modes of cantilever vibration. The quality factor associated with these four modes has been analytically calculated and compared with the theory proposed by Z. Hao et al. [64]. The increase in the quality factor is found to be limited by the support loss of the beam when using higher order modes. Fully loaded and end loaded cantilevers exposed to precise concentrations of Hg show significant shifts in the higher order modal frequencies while the fundamental mode does not show an appreciable shift under the same experimental conditions. For both fully loaded and end loaded cantilevers with repeated Hg exposures, the deflection signal does not saturate for the conditions studied. However, the shifts observed in the higher order modes seem to saturate with further exposures. The frequency shift for the 4^{th} order mode for a total exposure of 300 seconds to approximately 15 ppb Hg in N_2 is found to be -320Hz and -70Hz for the first and second cases respectively.

Chapter 5

COMPARISON OF HG SENSING BEHAVIOR OF AS DEPOSITED SPUTTERED AND THERMALLY EVAPORATED AU FILMS WITH CANTILEVERS

In this chapter a study is presented wherein both the as deposited sputtered and thermally evaporated Au films are employed for studying the Hg adsorption. [85] The bending and shifts in the thermally induced higher order modes are monitored as a function of total Hg exposure. It is found that depending upon the surface morphology of the films, the response of the higher order thermal cantilever modes to Hg changed.

5.1 Sputtered and Thermally Evaporated Au Films: Sensing Response

For sputter deposition of 5nm Cr and 50nm Au on one surface of cantilever, a Denton Discovery 18 system is used where the base pressure was $5X10^{-6}$Torr. For thermal evaporation of 5nm Cr and 50nm Au on one surface of cantilever, a CVC thermal evaporator (CVC Products, Inc.) is used where the base pressure was $2X10^{-6}$Torr. The cantilevers are transferred to the gas chamber following the Au deposition and are studied for their Hg response.

Cantilevers with sputtered or thermally evaporated films are exposed to four 100sec Hg exposures as shown in Figure 5.1. In Figure 5.1(a) and (b) the cantilever deflection and the Hg concentration as monitored by the Jarome Hg detector (Arizona Instruments) are plotted on the y-axes for sputtered and evaporated Au films respectively.

With the sputtered films, the deflection response of the cantilever always stabilizes after the Hg is turned off whereas with thermally evaporated films it shows an exponential decay after the Hg exposure is stopped. The deflection response in both the cases indicates that the cantilever bends away from the Au surface and hence the resultant surface stress is tensile in nature.

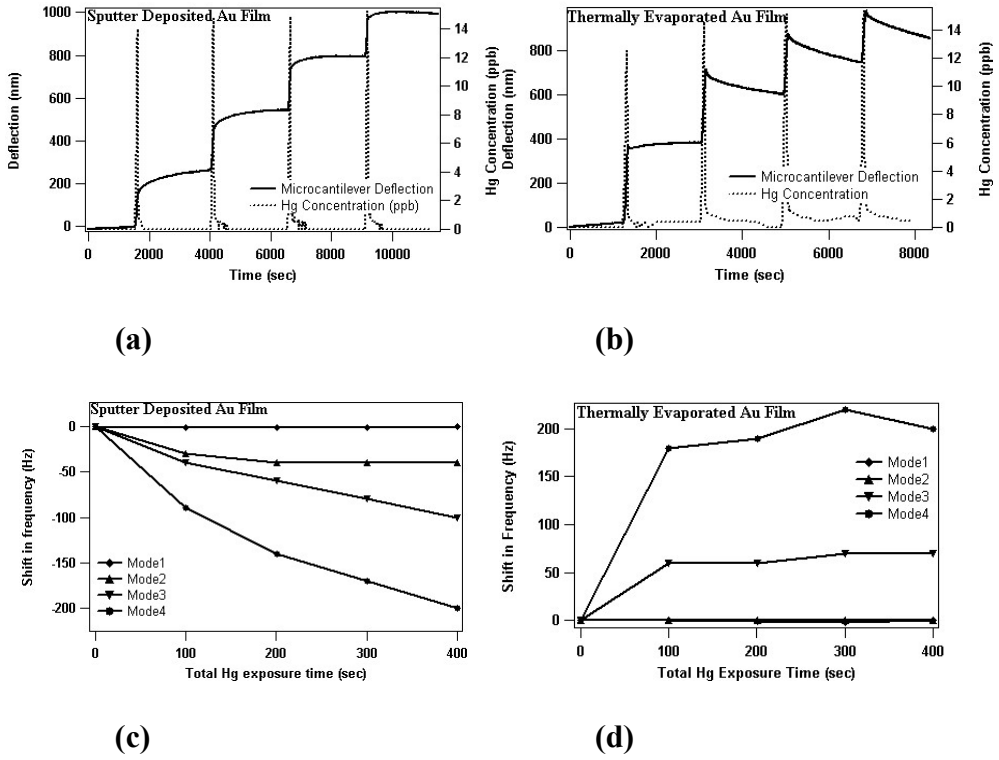

Figure 5.1 Cantilever deflection and shifts in the thermal modes after Hg exposures when Au is sputter deposited (a) and (c); and when Au is thermally evaporated (b) and (d) respectively

The shifts observed in the modal frequencies of the first four thermally induced modes as a function of total Hg exposure time are plotted in Figure 5.1(c) and (d) for

sputtered and thermally evaporated films respectively. It is seen that the spectral shifts are negative for sputtered films and are positive for thermally evaporated films.

Moreover all the studied modes except the fundamental mode show response to Hg when the sensing Au film is sputter deposited. In contrast when using the thermally evaporated films, the lower order modes do not show reasonable response to Hg.

5.2 Sputtered and Thermally Evaporated Au Films: Explanation

In order to understand this behavior, comparative analysis of the two Au surfaces is carried out, which is as follows. Here the differences between the two Au surfaces are presented before and after a large Hg exposure. Figure 5.2 (a) and (b) shows the scanning electron microscope images of the cantilevers with sputtered and thermally evaporated Au surfaces respectively. The atomic force microscope images of the two film surfaces are shown in Figure 5.2 (c) and (d) respectively. Comparing the two film surfaces, it is seen that the average grain diameter of the sputtered film surface is much smaller than that of the thermally evaporated film surface. Also the surface roughness value taken at random areas of sputtered film is smaller than that of the thermally evaporated film. (Note the image roughness of thermally evaporated Au film is 3 times that of the sputter deposited Au film (Figure 5.2 (c) and (d)).

Now assuming the Hg adsorption starts at the crevices of these different diameter Au surface grains, the Hg coverage on the sputtered film would be more continuous than that on the thermally evaporated surface.

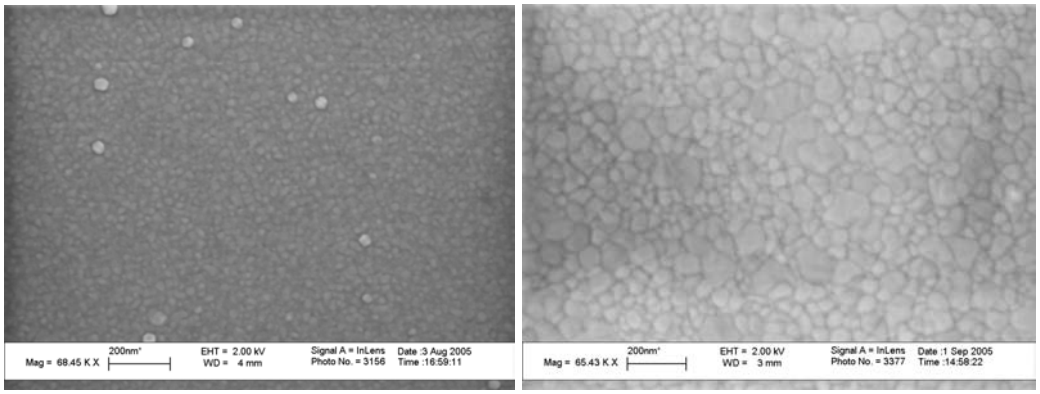

(a) **(b)**

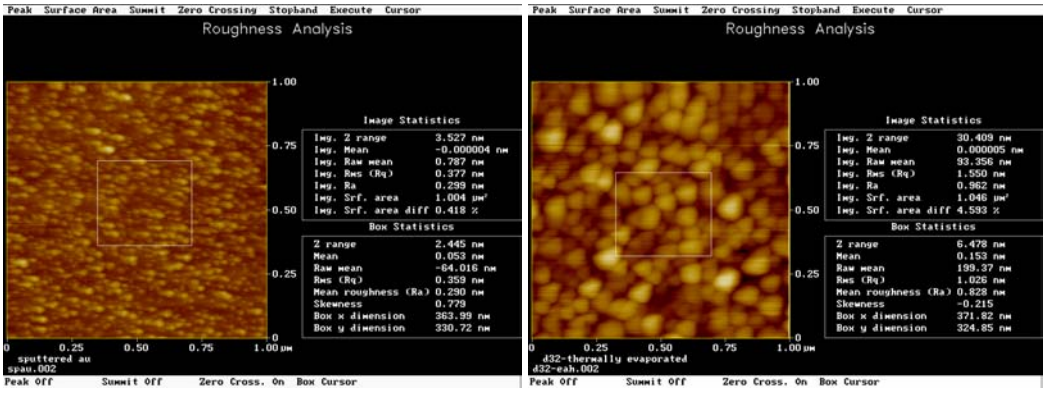

(c) **(d)**

Figure 5.2 (a) Scanning electron microscope image of as deposited sputtered Au film, (b) Scanning electron microscope image of as deposited thermally evaporated Au film, (c) Contact mode atomic force microscope images of a randomly selected surface on a cantilever of as deposited Sputtered Au film and (d) Contact mode atomic force microscope images of a randomly selected surface on a cantilever of as deposited thermally evaporated Au film

To see if this point is true, two different cantilevers, one with sputtered Au film and the other with thermally evaporated Au film, were exposed to 22ppb Hg for 1hr. The Hg exposed Au films on the cantilever surface were then studied under a scanning

electron microscope as shown in Figure 5.3. Both the sputtered (Figure 5.3(a)) and thermally evaporated (Figure 5.3(b)) Au films show a change in their surface morphology; however, the surface change for the sputtered film is more continuous than for the thermally evaporated one. Thus the uniform coverage of adsorbed Hg on the sputtered film adds more resultant mass to the cantilever surface and as a result the different modes show a decrease in their frequencies. In the case of the thermally evaporated films, because of the non uniform Hg coverage associated with the relatively large diameter of the surface grains (Figure 5.3(b)), the stress between the surface grains increases and as a result the different modes show an increase in their frequencies. This surface stress increase thus should be sufficient to cause the observed increase in the higher order modal frequencies but small enough to cause the cantilever to deflect in the same direction as that of the sputter deposited films. This small yet significant surface stress may be responsible for the instability of the deflection response after the Hg exposure is stopped in the case of the thermally evaporated films; however, more detailed studies are needed to support this statement.

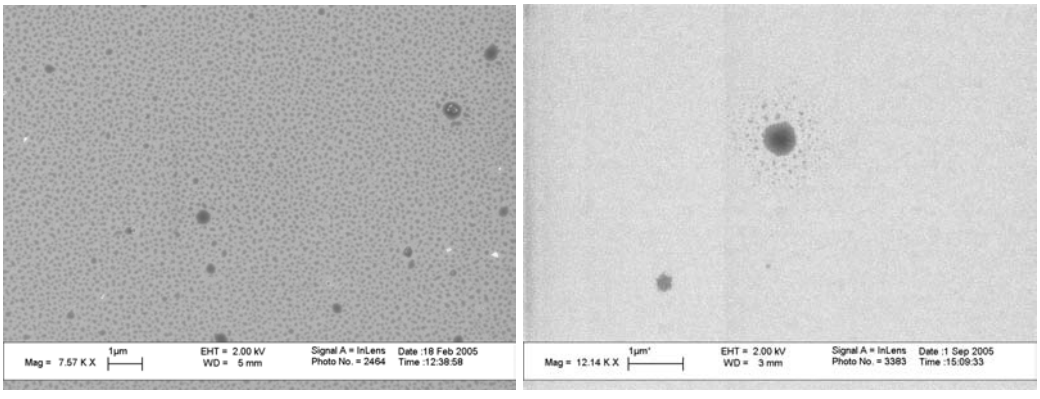

(a) (b)

Figure 5.3 Scanning electron microscope image of (a) Sputtered Au film, (b) Thermally evaporated Au film after 1hr Hg exposure.

In order to check if the spectral response of thermally evaporated films to Hg exposures is constant, four different cantilevers from two different cantilever batches are studied under the identical conditions for Hg exposures. The shifts observed in their modal frequencies are plotted as a function of the mode order as shown in Figure 5.4. The important point here is that all cantilevers show positive frequency shifts and the higher order modes show better Hg response. The inconsistency seen between the Hg responses of cantilevers from the two different batches is believed to be associated with different cantilever thicknesses mainly because the spring constant of the cantilever is a sensitive function of its thickness. The mean cantilever thickness for Batch1 (solid line) measured with scanning electron microscope is 1.44μm whereas that for Batch2 (dashed line) is 1.32μm.

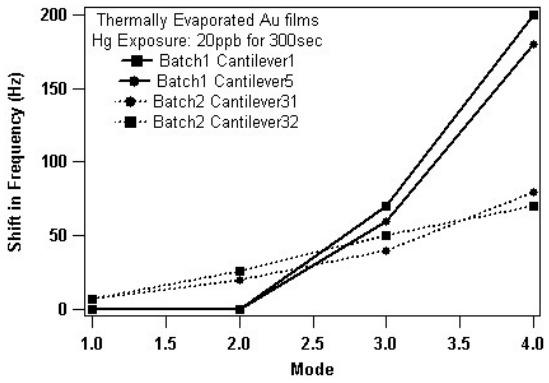

Figure 5.4 Shift in the thermally induced flexural modes of cantilevers from different batches after 200ppb Hg exposure for 300sec. Note the consistency in shifts between cantilevers within a batch, but not between different batches

5.3 Sputtered and Thermally Evaporated Au Films: Spectral Hg Response Vs Percent Au Coverage

In order to check if all cantilevers with thermally evaporated Au films show an Hg spectral response similar to those with sputtered Au films, fourteen different cantilevers from Batch1 are studied for their spectral shifts as a function of % Au coverage. Seven cantilevers were deposited with sputtered Au films and the other seven with thermally evaporated Au films. The Au was then etched with photoresist etch mask on all the cantilevers so that each one has a specific Au coverage (Figure 5.5) [82]. Each of these cantilevers was exposed with 22ppb Hg for 600sec. The spectral data is recorded 1000sec after the Hg exposure is stopped.

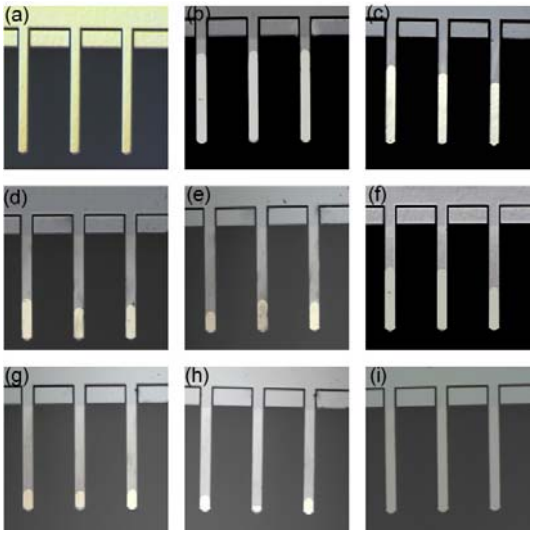

Figure 5.5 Optical microscope images of three cantilevers with various Au coverage achieved by subsequent wet Au etching. (a) 5nm Cr, 50nm Au coated cantilever, (b)-(h) the same cantilevers after subsequent Au etch steps and (i) bare Si cantilevers

The shift in the thermally induced modes with Hg exposure is plotted as a function of % Au coverage in Figure 5.6. The trend of the spectral response for the cantilevers with sputter deposited Au film (Figure 5.6(a)) is found to be opposite to those with thermally evaporated film (Figure 5.6(b)). It can be clearly said from Figure 5.6(a) that for cantilevers with sputter deposited Au films, the nature of the higher order modal frequency shifts, after Hg adsorption, strongly depends upon the fractional Au coverage. All the thermal modes except the 1st order mode show reasonable shifts with Hg exposures for all the Au coverage studied here. But for cantilevers with thermally evaporated Au films, reasonable spectral response with good signal to noise ratio (Figure 5.6(b)) is observed only for the 4th order mode. The nature of the spectral response as a function of % Au coverage and its implications are currently being studied by considering a mechanical model. For now from Figure 5.6 it can be said that for thermally induced spectral studies with cantilevers, the thermally evaporated Au film is not as sensitive as the sputtered Au films when deposited on one of its surface.

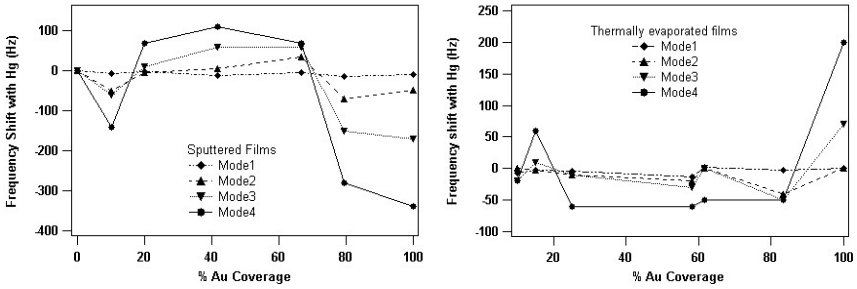

(a) **(b)**

Figure 5.6 Frequency shift with Hg exposure versus % Au coverage for (a) sputtered Au films and (b) thermally evaporated Au films

5.4 Conclusions

As deposited sputtered and thermally evaporated Au films are studied for Hg response with cantilevers, it is seen that although the bending direction of the cantilevers with the two kinds of Au films is the same, the deflection response for thermally evaporated Au films after Hg exposure is stopped tends to decay. The thermally induced spectral studies of cantilevers reveal that the surface morphology of the Au film plays an important role in modifying the flexural frequencies of the cantilever vibrations. However one needs to use the 4^{th} order mode for studying surface interaction of Hg with thermally evaporated Au films. On the contrary, with sputtered Au films, all but the 1^{st} order thermal mode show reasonable response to Hg. Thus it is concluded that as deposited sputtered films are more sensitive to Hg exposures than as deposited thermally evaporated films when studied using thermally induced higher order modes of cantilever vibration. This conclusion is further supported by studying cantilever spectral response as a function of % Au coverage with sputter deposited and thermally evaporated Au films.

Chapter 6

CHARACTERIZATION OF GOLD FILMS

The results of the various surface analysis techniques used to study the Hg exposed Au surfaces of cantilevers are presented in this chapter. SEM and AFM studies are carried out to understand morphological changes occurring at the Au surface due to Hg interactions and are presented in Section 6.1. Thin film X-ray Diffraction (XRD) and Energy Dispersive Spectroscopy (EDS) studies are carried out to find out the presence of Hg on the Au surface and are given in Section 6.2. The presence and weight percentage of Hg is precisely found out by X-ray Photoelectron Spectroscopy (XPS) and this data is also given in Section 6.2. The XPS depth distribution of Hg on the Au surface was found to be consistent with literature.

6.1 Morphological Changes of Au Surface upon Hg Exposure

The Au surface have been monitored before and after Hg exposures to observe any morphological changes associated with the adsorption of Hg on Au surfaces. A LEO 1550 field emission SEM and Digital Electronics' Dimension 3000 AFM have been used for these studies. Secondary electron images of the Au surface of the cantilevers are studied with the SEM and contact mode images on the cantilever surface are obtained with the AFM. Some of the images were presented in Section 5.2 which has helped in understanding the differences between the sputtered and thermally evaporated Au surfaces before and after Hg exposure. Clear surface morphological differences between

the two types of Au films were seen in Figure 5.2 where both SEM and AFM Au surface images were given prior to any Hg exposure. Please note that a triangular silicon nitrite cantilever with 0.06N/m spring constant was used to image the free standing beam as shown in Figure 6.1.

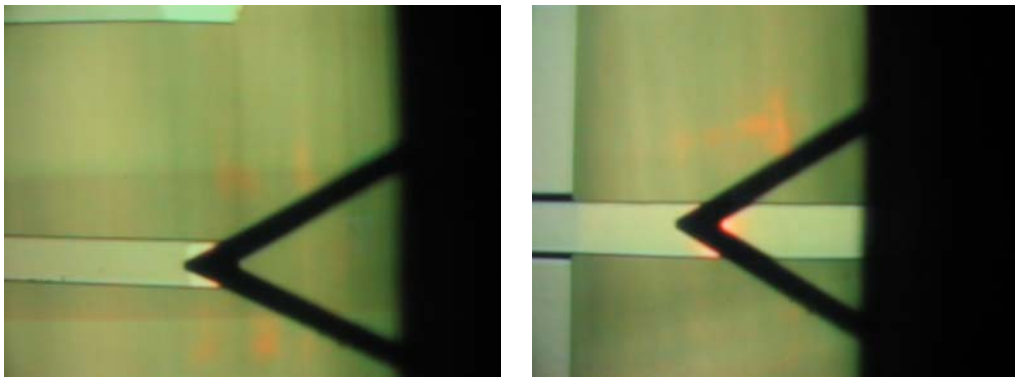

Figure 6.1 Optical pictures, where the triangular imaging tip is used to scan the Au surface of the cantilevers under study

Both the sputtered and thermally evaporated Au film surfaces are then exposed to same concentrations of Hg and are studied with SEM as shown in Figure 5.3. A more uniform surface coverage upon Hg exposure is observed for sputtered Au film than the thermally evaporated Au film.

Furthermore the Hg exposed films are studied with AFM at various times after exposure to Hg. It is seen from Figure 6.2 that the Au surface changes due to rearrangement of Hg over time. This observation is found consistent with those of others [92, 93].

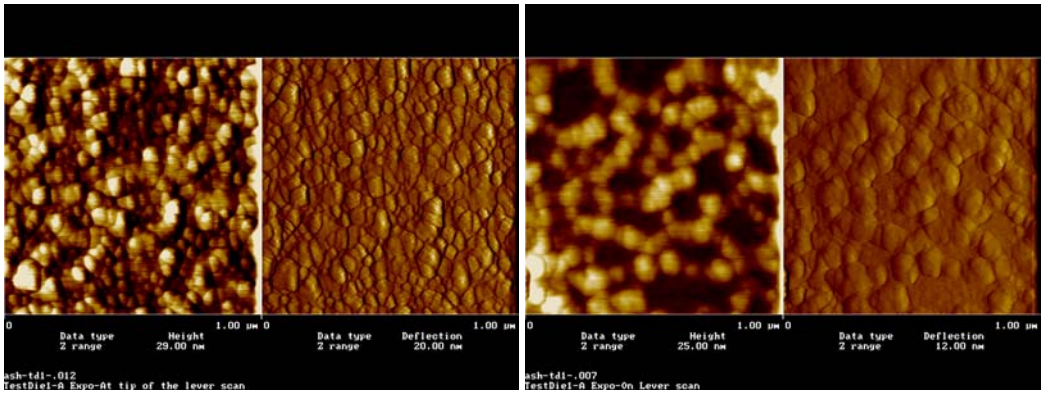

(a) **(b)**

Figure 6.2 Contact mode AFM (height image on left and deflection image on right) images of Au surface (a) right after Hg exposure and (b) 24 hours after the Hg exposure

Thus from the SEM and AFM studies, it is seen that the Hg adsorption process shows different trends for the sputtered and thermally evaporated Au films depending on their initial surface morphology. Also it is observed that the Hg rearranges on the surface and with time (for 24 hours, greater than the time scale for the sensing experiments) the morphology of the surface changes.

6.2 Compositional Changes of Au Films upon Hg Adsorption

XRD, EDS and XPS studies are carried out in order to get an estimate of the amount of Hg on the Au surface after exposure.

XRD Analysis

For the XRD studies, a Rigaku thin film X-ray diffractometer is used. The cantilevers were studied before and after Au deposition and after four Hg exposures of 15ppb concentrations for 100sec with Cuk_{α} radiation and the XRD spectra are shown as various sample stages in Figure 6.3.

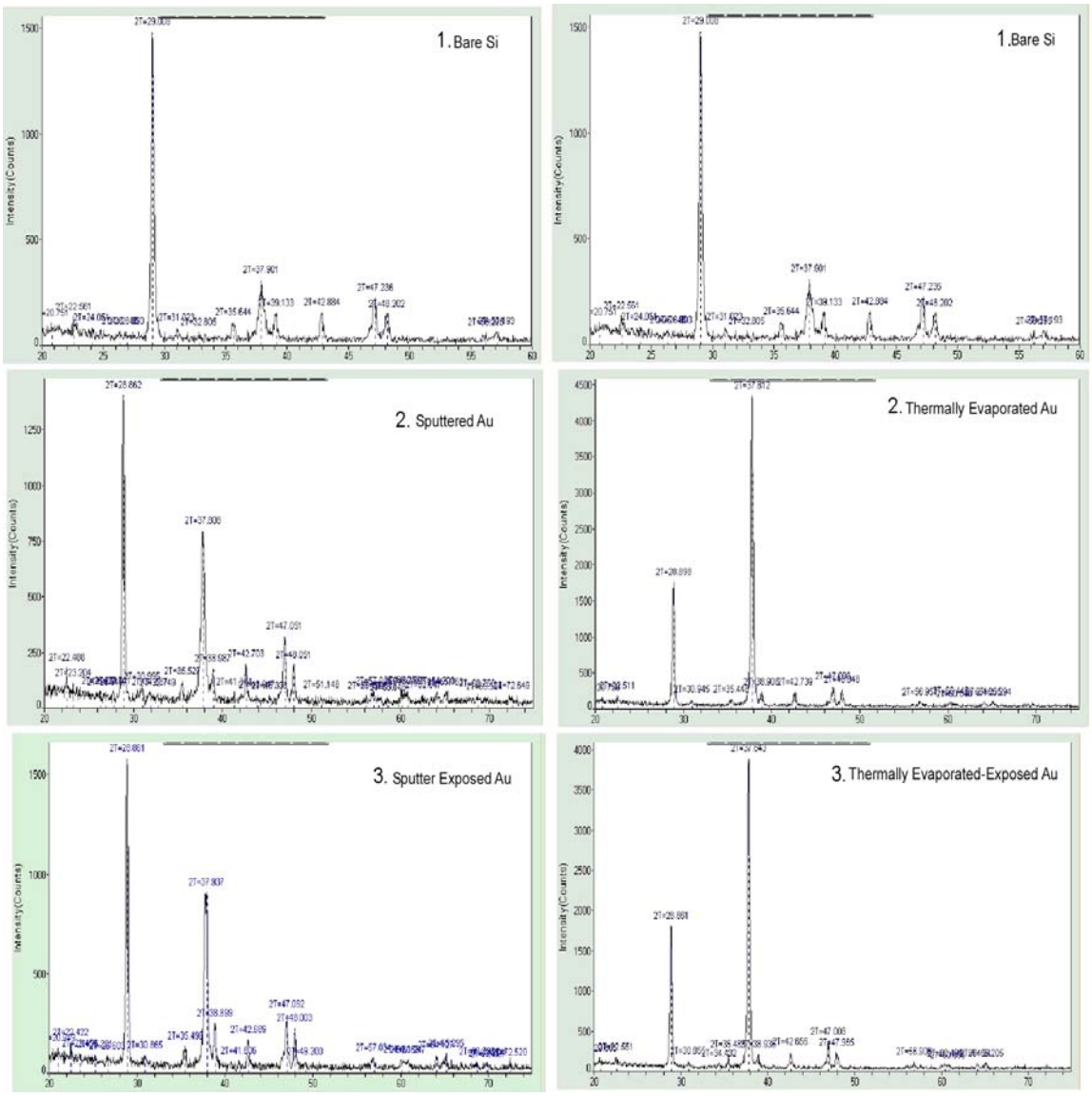

(a) **(b)**

Figure 6.3 XRD spectra for cantilevers at various stages. (1) Bare Si cantilevers, (2) After Au deposition and (3) After Hg exposure for (a) sputtered and (b) thermally evaporated Au films

The XRD studies failed to show any Hg related information. This was thought to be associated with the small amount of Hg adsorbed on the Au surface during these pulsed exposures of low Hg concentrations. Please note that the Au <111> peak for the thermally evaporated films is double the intensity of that for sputtered Au film. Thus the degree of crystallinity in the thermally evaporated films is more than that of the sputtered films.

EDS Analysis

The cantilevers were then studied with an EDS system (Make Princeton Gamma Tech) installed on the LEO 1550 SEM.

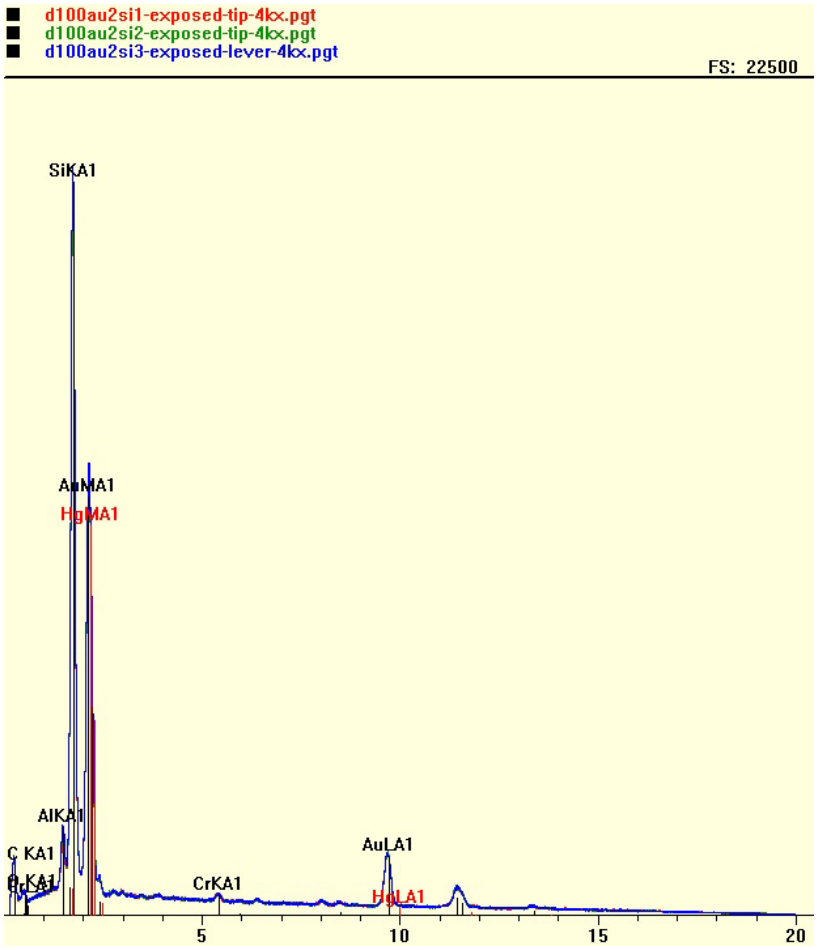

Figure 6.4 An EDS spectrum of a cantilever after Hg exposure

Figure 6.4 shows the EDS spectrum of a cantilever after Hg exposure. The presence of Hg on the exposed cantilever surface is evident from this spectrum. But the weight percentages given were not reliable because the X-ray transition energies of Au and Hg are very close to each other, making the peak overlap as seen in the spectrum, thus the quantitative analysis becomes ambiguous.

XPS Analysis

XPS analysis of the unexposed and exposed samples was carried out using a commercial foundry service. The XPS data were acquired using a probe beam of focused, monochromatic Al K_α radiation.

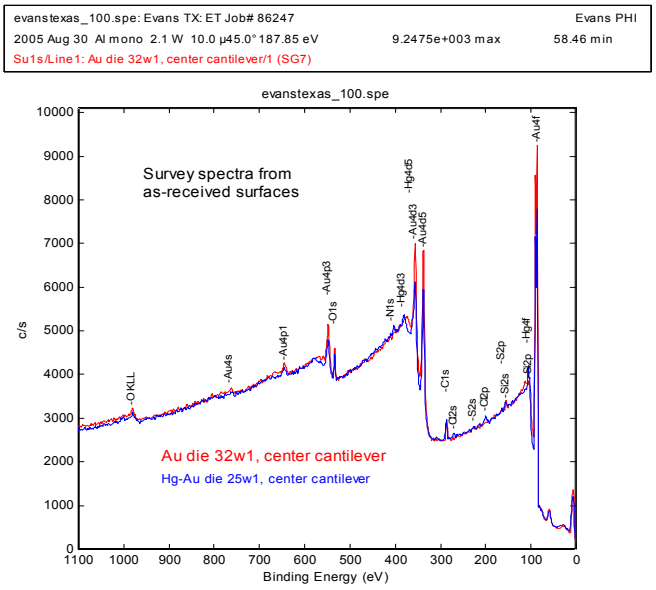

Figure 6.5 Survey spectra of unexposed (red line) and Hg-exposed (blue line) Au surface of a cantilever

The x-rays generate photoelectrons that are energy analyzed and counted to reveal the atomic composition and chemistry of the sample surface. The escape depth of the photoelectrons limits the depth of analysis to the outer ~50 Å. The data presented in Figure 6.5 shows low resolution survey scans for exposed and unexposed cantilever samples, which give the full spectrum between 0 and 1100eV binding energy.

High resolution Au4f and Hg4f spectra (Figure 6.6) were collected to obtain the Hg:Au ratio, since the Hg peaks overlap secondary peaks associated with Au. The surface ratio of Hg to Au was about 0.08. See the atomic concentration Table 6.1 for other details of the surface compositions.

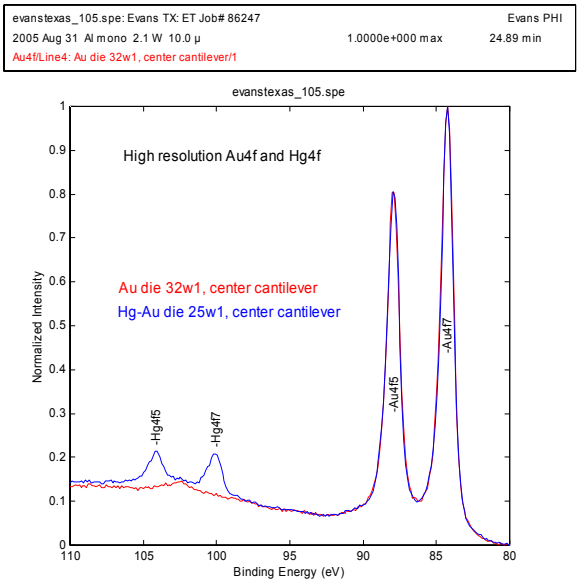

Figure 6.6 High resolution XPS spectrum of unexposed (red line) and exposed (blue line) cantilever Au surface.

Table 6.1 XPS Surface concentration (Atomic %)

Sample	C	N	O	Si	S	Cl	Au	Hg
Au die 32w1, center cantilever	29.9	-	21.5	6.6	1.7	-	40.5	-
Hg-Au die 25w1, center cantilever	35.8	6.3	16.6	3.5	1.5	2.1	31.7	2.6

A depth profile was obtained, as shown in Figure 6.7, from the Hg-exposed sample to assess the depth of Hg penetration. The profile is presented with minutes of sputtering as the x-axis. The ion beam conditions used give an SiO_2 sputter rate of 35Å/min, but the sputter rate for Au varies with deposition conditions and can range from two to four times faster than the SiO_2 rate. Assuming that the expected Au layer thickness of 500Å, the sputter rate in this Au coating was ~90Å/min.

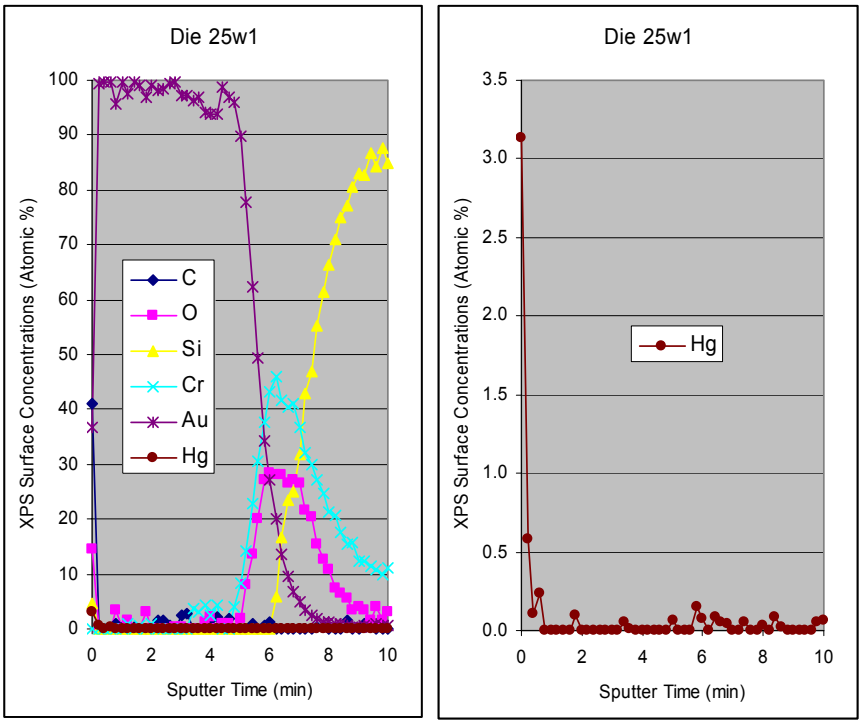

Figure 6.7 XPS depth profile of the Hg exposed cantilever sample

Hg was detected on the non-sputtered surface and after the first 0.2 minute sputter cycle, but was below detectable levels by 0.4 minutes of sputtering. Assuming 90Å/min as the sputter rate, this indicates that Hg was only present at detectable levels in the upper ~35Å of the Au film. The Hg detection limit was about 0.2 atomic percent for the conditions used. Note that detection limits for the lighter elements were much higher. The apparent spikes of C and O within the Au portion of the profile are attributed to "noise" since the detection thresholds were on the order of a few atomic percent for those elements.

6.3 Conclusions

The detailed results of various characterization techniques employed to study the Au surface are given in this chapter. With the help of SEM and AFM images, an explanation as to why sputtered and thermally evaporated Au films show a different higher order modal response is given in Section 6.1 with the help of Section 5.2 to avoid duplication of these results. Also AFM images, on the Au surface taken right after a Hg exposure and 24 hours after the same Hg exposure shows experimental evidence of rearrangement of Hg on the surface. The XRD data shows that the thermally evaporated films are more crystalline than the sputtered films; however, no evidence of Hg on the surface is found with this technique. This was attributed to the very small concentration of Hg on the cantilever surface. The EDS analysis confirmed the presence of the Hg on Au surface; however, reliable weight percentage information was not obtained due to Au-Hg peak overlap. XPS analysis gave a detailed picture of the presence of Hg on the Au surface and the depth to which it is present is approximately 35Å.

Chapter 7

STUDY OF THERMALLY INDUCED MICROCANTILEVER MODES AS A FUNCTION OF SENSITIZING COATING COVERAGE

In this chapter, study of the thermally induced fundamental and three higher order modes of rectangular Si cantilevers as a function of coverage of the sensitizing coating to establish a baseline for cantilever behavior is presented. The sensitizing coating chosen here is Au film, mainly because of its use in many biological sensing applications with cantilevers. The results of this study are not clearly understood at this point, but they are presented here due to their potential and uniqueness to understand the mechanical property changes of cantilever.

7.1 Motivation

As has been discussed in the previous chapters, to use a cantilever as a sensor, a sensitizing coating is typically applied on one of its surfaces. For sensitive mass detection, shifts in the externally excited fundamental frequency are monitored. The variation of mass along the length of the cantilever upon analyte interaction is considered responsible for the observed frequency shifts. However changes in the spring constant of the cantilever with the analyte interaction raises questions about the calculated adsorbed mass, especially when the active sensitizing coating is applied along the entire length of the cantilever due to the frequency change associated with spring constant changes. Early literature indicates that by using sensitizing coating at the free end of the cantilever, a

purely mass loading dominant response is achieved. Recent experimental efforts propose simultaneous study of the resonance frequency and/or cantilever deflection to get fairly accurate mass sensing results. However no efforts have been carried out to study the frequency response of a cantilever as a function of the fractional coverage of the sensitizing coating except for fully loaded and end loaded cases. Here using the end loading process described in Chapter Four, the study of frequency shifts of the first four flexural modes of cantilever vibration is carried out as a function of the Au coverage. This is done to check if the cantilever's mechanical property changes can be seen when the spectral response is studied with variation in Au coverage. Also, understanding these results may give an insight into where exactly along the cantilever length the sensitizing coating should be placed in order to get optimum mass loading response without any interference from spring constant changes. This data may also be useful to understand which mode of the cantilever should ideally be used for mass sensing. Given the random origin of the chemical interaction on the sensitized surface on cantilever, this data can further be studied extensively to understand the sensitizing coating's geometry specificity towards its analyte.

7.2 Spectral Study as a Function of Au Coverage

Three different cantilevers are used to study the spectral response as a function of percent Au coverage and are shown in Figure 5.5. A bare Si cantilever is first sputter-deposited with 5nm Cr and 50nm Au (Figure 5.5(a)), and its spectral response is measured. To vary the percent Au coverage on one surface, a simple technique, as outlined in Section 4.3, is used where the sputtered Au is selectively etched from the fixed end towards the free end of the cantilevers [82]. Using this technique, the Au coated

cantilevers are wet etched in a number of steps. The optical microscope images at subsequent etch steps are shown in Figure 5.5 (b)-(h).

After each etch step, the cantilever is transferred to the gas chamber and the spectral data is taken. At the last etch step (Figure 5.5 (i)) the Au and Cr is altogether stripped off of the cantilever surface and the spectral data is taken.

The frequency response of the first four thermally induced modes as a function of percent Au coverage on one surface of the cantilever is shown in Figure 7.1 (a)-(d) respectively. Here the 0% Au coverage indicates a Si cantilever and 100% Au coverage means cantilever deposited with 5nm Cr and 50nm Au along the entire length of one surface.

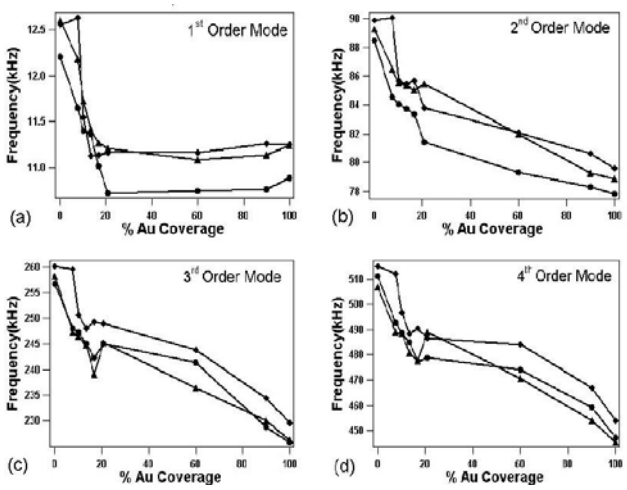

Figure 7.1 Frequency versus the percent Au coverage along the cantilever length for the first four modes (a)-(d) respectively. Three lines in each plot represent the data from three different cantilevers as shown in Figure the 5.5

The vibration frequency of the nth cantilever mode can be written as,

$$f_n = \frac{1}{2\pi}\sqrt{\frac{k}{m_{eqn}^{*}}},$$

where, k is the spring constant and m_{eqn}^{*} is the equivalent microstructure's mass for the considered mode. So the changes in the modal frequencies of a cantilever with various coverage of Au can result from the combination of mass change and variation in spring constant. As seen in Figure 7.1, all four modes of the cantilevers show a decrease in frequency when 20% of its free end is coated with Au, indicating that the change in spring constant is negligible in this region and the changes in modal frequencies are entirely the result of mass loading. The second and higher order modes continue to show decrease in their frequency (Figure 7.1 (b)-(d)) when the Au coverage is further increased till 100%; however, the rate of frequency change is rather different than that during the first 20% Au coverage. This rate change is considered an indication that changes in spring constant along with changes in mass loading are responsible for the resultant changes in the modal frequencies. Also note that for the fourth order mode in Figure 7.1 (d), the slope of the curve further changes after 80% Au coverage. The fundamental mode in Figure 7.1 (a) shows almost no frequency change after the first 20% Au coverage and this is possibly due to the change in frequency due to mass loading being balanced by the counteracting change in frequency due to spring constant change.

Although we present this simple explanation, the response in Figure 7.1 shows a complex nature. Understanding these results may give an insight into where exactly along the cantilever length the sensitizing coating should be placed in order to get optimum

mass loading response without any interference from spring constant changes. This data may also be useful in understanding which mode of the cantilever should ideally be used for mass sensing. A mechanical model to understand this behavior is necessary which opens up the future work of this research.

7.3 Conclusions

In this chapter, a study of the thermally induced flexural spectrum of rectangular Si cantilever with respect to percent Au coverage is presented. The motivations behind this study are presented along with their implications. The results of the study are presented and a simple explanation is given to explain the data. However it is understood that a rigorous model is needed to understand the full potential this data holds. Due to the novelty and potential associated with this study, it is presented here as a chapter; however, it is also acknowledged that this chapter does not give complete insight into the data presented.

Chapter 8

SU-8 MICROCANTILEVER FABRICATION AND TESTING

In this chapter the fabrication process development for fabricating rectangular polymer cantilever is given. The polymer chosen here is SU-8 which is a photoepoxy polymer well used in the microfabrication industry as a negative photoresist. The details of this material and the fabrication process are given in Section 8.1. The so fabricated SU-8 cantilevers are tested for Hg vapor and those results are given in Section 8.2.

Motivation

It has so far shown in the previous chapters that thermally induced higher order modes can be used for sensing using rectangular Si cantilevers. It is also shown that large sensing response is achieved when the highest detectable mode is used for sensing. This is in agreement with the scaling law defined in Chapter Two. In the case of Si cantilevers, the highest mode detected with reasonable signal to noise ratio is the fourth order mode which falls approximately at 450 kHz. Also as the mode order increases, the amplitude of the mode goes down. When compared with the externally excited fundamental mode, the Q factors associated with the thermally induced modes are very small. Given these factors, using a flexible material for cantilever fabrication to check if such a cantilever can have a richer thermal spectrum with more flexural peaks of vibration is proposed. If so, the idea proposed is to check if the highest order mode shows better response than the fourth order mode studied here for Si cantilevers. Other advantages of fabricating and

studying polymer cantilevers are low cost, cantilever array production and flexibility in geometry modifications.

8.1 Polymer Cantilever Fabrication

This section covers topics including the choice of the material (Section 8.1.1) and the fabrication process for SU-8 cantilevers (Section 8.1.2).

8.1.1 Choice of the Material

Various polymer materials were investigated for cantilever fabrication owing to their specific material properties. Poly(vinylidene fluoride) (PVDF) [86] was the first material considered because it is a piezoelectric polymeric material with the modulus of elasticity of 2.5GPa. This material needs to be polled to be piezoelectric and is commercially available in the form of films of various thicknesses with minimum thickness being 1mil. Back of the envelop calculations were performed to get an estimate of output voltage levels given the nanometric deflection of the cantilevers. The voltage levels were found to be in micro-volt range which indicated that the electronics needed to be quite powerful to get good signal to noise ratio with these cantilevers. Also it was found that the piezoelectric properties of PVDF are reported to be less than optimum when operating under DC, a condition which is desired for thermal spectrum studies. Given these factors and the fabrication difficulties associated with working with non-polled liquid polymer mixtures, this material was discarded for the fabrication of polymer cantilevers.

The second polymer considered was Liquid Crystal Polymer (LCP) [87] which also is commercially available in the form of films of various thicknesses, the minimum being 25μm. This polymer has a Young's modulus value from 1.3 – 4 GPa. As shown

in reference [87], the fabrication process seemed simple for this polymer; however, many attempts to bond the LCP film to Si and glass substrate did not yield any success. Thus this polymer was discarded.

The third polymer sought to be a material for cantilever was SU-8. SU-8 is an epoxy-based negative photoresist which gets cross linked upon UV exposure. It has a high chemical resistance which makes it a suitable component material. The resist is compatible with conventional microfabrication techniques, and it is relatively easy and fast to process. The use of SU-8 for MEMS processing is growing exponentially in recent years, one example of such is microfluidic devices. Also AFM probes [88], cantilevers with integrated strain gauge readout in a microfluidic system [89, 90], and passive cantilevers for DNA detection [91] have been fabricated in SU-8. It is shown that SU-8 cantilevers show fundamental mode of vibration and the deflection response of these cantilevers is five times better than Si or silicon nitrite cantilevers [91]. However the thermal spectral studies are not reported on SU-8 cantilevers.

Two different commercial (Microchem Corp.) formulations of SU-8 are used for the fabrication of cantilevers. The first one is SU-8 2001 which gives a thin (1-2μm) film after spin coating and the other is SU-8 2100 which gives a thick (100-260μm) film after spin coating.

8.1.2 SU-8 Cantilever Fabrication Process

The fabrication process flow is shown in Figure 8.1. A silicon wafer is used as a handle/support wafer during the fabrication process. First a 5nm Cr/ 50nm Au / 50nm Cr layer is sputter deposited which is used as the release layer for SU-8 structure. Then the alignment marks are transferred for subsequent alignment of two photolithographic steps.

A 1.6μm thick SU-8 layer is spun on top of the wafer and baked on hotplate at 65^0C for 1 minute and then with a ramp to 95^0C for 3 minute.

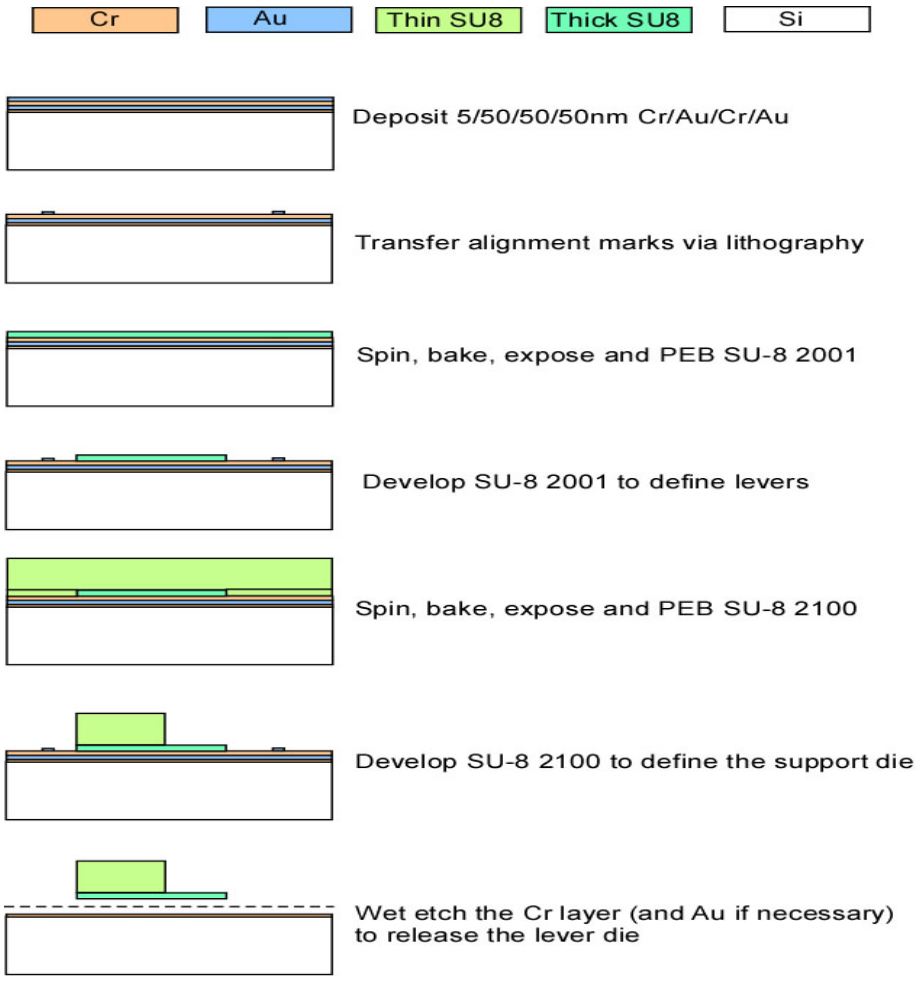

Figure 8.1 Fabrication process for SU-8 cantilevers

The cantilever geometry is then transferred onto this SU-8 layer with a photolithographic process by exposing the SU-8 with a UV dose of 95mJ/cm^2 through the SU-8 cantilever definition mask. To further promote the cross linking of the SU-8, it is baked after exposure for 1 minute at 65^0C and 1 minute at 95^0C. The non cross linked

SU-8 is removed by immersing the wafer in the developer (propylene glycol monomethyl etcher acetate, PGMEA) solution for 1 minute. The 250μm thick SU-8 layer is then spun on top of the wafer to define the support for the cantilever dies. The thick SU-8 is softbaked for 15 minutes at 65^0C and 35 minutes at 95^0C. The wafer is then exposed through the die definition mask to an UV exposure dose of 450mJ/cm^2. The SU-8 is then further baked at 65^0C for 1 minute and at 95^0C for 15 minutes to promote the cross linking. The non cross linked SU-8 is then removed by immerse-developing the wafer in PGMEA solution.

Both the defined SU-8 layers, before the release, are then hardbaked on hotplate at 65^0C for 1 minute, 95^0C for 5 minutes and 195^0C for 15 minutes. The wafer is placed on the hotplate during the ramping of the temperatures. This hardbake process ensures that most of the SU-8 is fully cross linked. In this form it is chemically very stable and resistant to other chemicals. The SU-8 structure is released from the handle Si wafer by wet Cr etching. A SEM image of a released SU-8 cantilever die is shown in Figure 8.2.

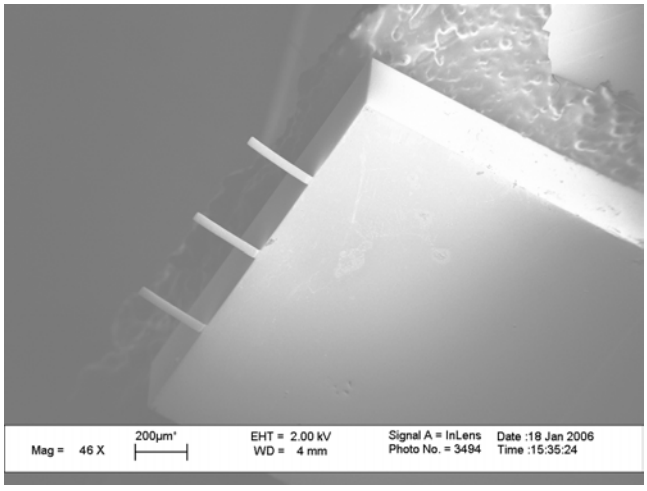

Figure 8.2 A SEM image of a released SU-8 cantilever die

The SU-8 cantilevers are sputter deposited with Au for the Hg sensing studies after they are released from the handle wafer. The thickness of Au has been optimized so that the cantilevers do not bend after the deposition.

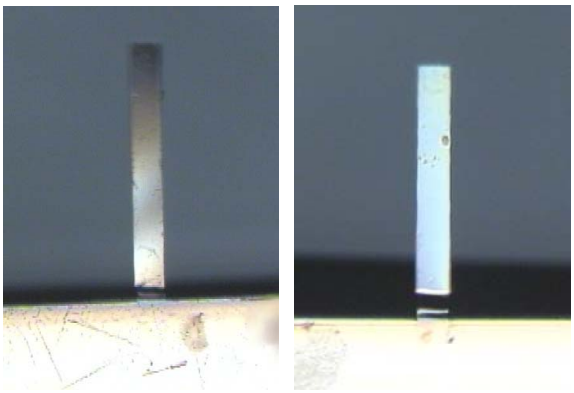

(a) **(b)**

Figure 8.3 SU-8 cantilevers after Cr/ Au deposition of (a) 3nm Cr and 30nm Au and (b) 2.5nm Cr and 25nm Au. Note that the cantilever in (b) is not bent where the one in (a) is relatively bent after the deposition.

A maximum thickness of 2.5nm Cr/ 25nm can be sputter deposited on one surface of these cantilevers without any bending, which is illustrated in Figure 8.3 with the help of optical microscope images. This thickness of the Au films is used for the Hg sensing studies presented in the next section.

8.2 SU-8 Cantilever Testing

The as deposited SU-8 cantilevers are transferred to the gas chamber to study their thermal spectrum. A distinct spectral characteristic is observed for the SU-8 cantilevers with the same lateral dimensions as their Si counterparts (300μm long, 35μm wide). The thicknesses of Si cantilevers studied ranged from 0.9μm to 1.5μm. The

thickness of the SU-8 cantilevers fabricated here is 1.6μm +/-0.5μm. A typical experimentally observed spectrum for SU-8 cantilever is shown in Figure 8.4 and is compared with the thermal spectrum of Si cantilever.

It can be noted that the modal frequencies of the SU-8 cantilevers is much smaller than the respective modal frequencies of Si cantilevers. Although a distinct spectral characteristic is observed for the SU-8 cantilevers, only the first four modes are visible for this geometry. So the first purpose of studying more mode orders with SU-8 cantilevers is not fulfilled with this geometry of SU-8 cantilevers. However given the fact that the four modes can be clearly seen with comparable amplitudes to their Si counterparts, these cantilevers are studied for Hg sensing response.

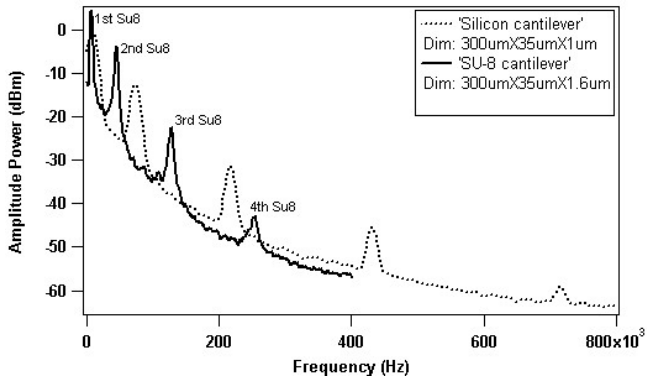

Figure 8.4 Comparison between thermally induced spectrum of SU-8 cantilever (solid line) with a Si cantilever (dotted line)

Before studying the Hg response, however, the spectral data of these cantilevers is verified to be the flexural modes of vibration by two different techniques as shown in Table 8.1.

Table 8.1 Comparison of the experimentally observed frequencies of SU-8 cantilevers with those obtained with different techniques

Mode	**Theoretically Calculated Frequency(Hz)**	**Frequency measured with active excitation with D3000 AFM (Hz)**	**Experimentally measured Frequency(Hz) (Observed Standard Deviation Hz)**
1	7,762	6,950	6,920 (6)
2	48,640	45,850	44,843 (25)
3	114,500	126,400	127,895 (200)
4	224,300	253,850	252,675 (400)

The standard deviations associated with the different modes which represent the noise associated with the spectral measurements are rather high with SU-8 cantilevers. This is expected because of the polymeric nature of these cantilevers. But with the same nature (i. e., the flexibility) of this material, it is expected that the spectral shift would be higher to get a good signal above this noisy floor.

The cantilevers are then studied for their deflection baselines, which take about four hours to stabilize to be within +/- 100nm per 1200 sec. This is a long time when compared to the Si cantilevers which take only 20 minutes to be within +/-50nm per 1200sec. This longer drift is mainly related to the laser heating which, owing to the low thermal conductivity of this polymer, takes longer to be at a thermal equilibrium.

The cantilevers are exposed to three exposures of 100 sec each to Hg concentration of 14 ppb.

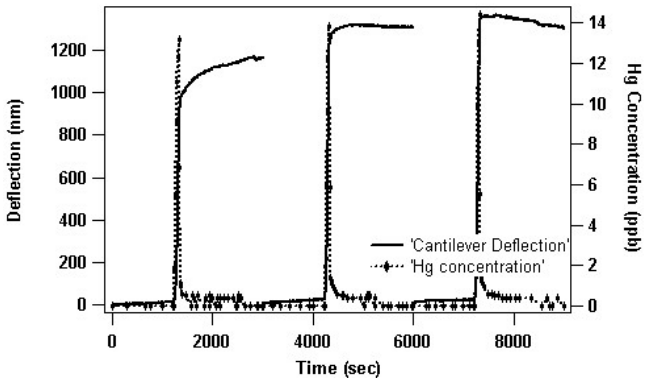

Figure 8.5 Deflection response of SU-8 cantilevers for three Hg exposures of 100 sec each

The deflection response to the Hg exposure is as shown in Figure 8.5, where deflection in nm and Hg concentration in ppb are plotted along the y axis. Comparing this response to Figure 4.2 (a), where the Si cantilever's deflection response is given, an order of magnitude increase in the deflection signal is seen for the SU-8 cantilevers. This can very easily be explained with the formula derived by Sader [26, 40] from equation (2.10) for cantilever deflection given below

$$z = \frac{3(1-\nu)L^2}{Et^2}(\delta\sigma_1 - \delta\sigma_2), \qquad 8.1$$

where E is the Young's modulus and ν is the Poisson's ratio of cantilever material, t and L are thickness and length of the cantilever and z is the cantilever deflection resulting from a differential surface stress change of $(\delta\sigma_1 - \delta\sigma_2)$.

The differential surface stress change is found to be 0.1749N/m calculated from the deflection data of Si cantilever. Now since Au-Hg interaction is a surface phenomena, assuming the same surface stress changes occur on the Au surface of SU-8 cantilever

after Hg exposure, the deflection of SU-8 cantilever should be approximately 1000nm. This value compares well to the experimental data as shown in Figure 8.5.

Now the spectral data of the same cantilever is as shown in Figure 8.6 where the shift in modal frequencies is plotted as a function of total Hg exposure time.

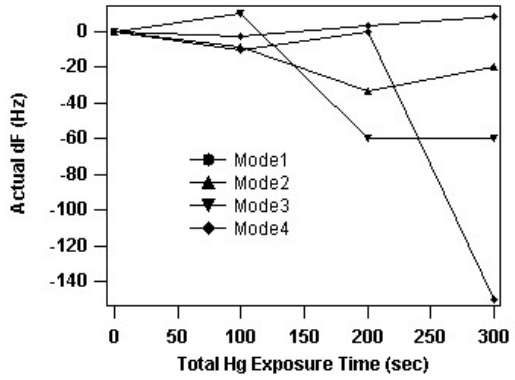

Figure 8.6 Observed shifts in the modal frequencies for SU-8 cantilever after Hg exposures

Given the standard deviations associated with each mode, there is no shift observed in any of the modes upon Hg exposures. Although disappointing, this result can be explained with equation (2.12) which says that larger frequency and smaller spring constant cantilever would give better sensing response. Here although we have lowered the spring constant [91], the modal frequencies are lowered too. Thus no improvement in the spectral sensing response is seen for the same dimensions of SU-8 cantilevers.

To check if this statement is entirely true, that is, higher sensing response is observed for higher modal frequencies, wider cantilevers with the same lengths and thicknesses are studied with Hg exposures. These cantilevers are 300μm long, 100μm wide and 1.6μm thick. The thermal spectrum of these cantilevers show six modes as shown in Figure 8.7.

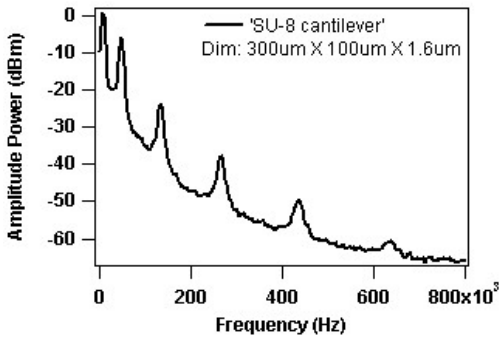

Figure 8.7 Thermal spectrum of a wider SU-8 cantilever. Note that this cantilever shows six modes of vibration

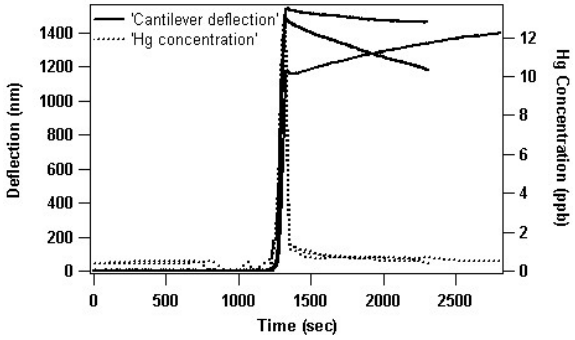

(a)

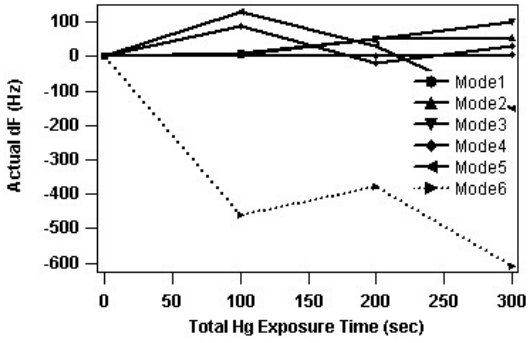

(b)

Figure 8.8 (a) Cantilever deflection and Hg concentration as a function of time and (b) Spectral shifts as a function of total Hg exposure time, of the wider SU-8 cantilevers

The cantilever deflection and spectral response upon three Hg exposures of 100 sec each is as shown in Figure 8.8. It is seen from Figure 8.8(b) the 6^{th} order mode with modal frequency 620 kHz shows some response to Hg. So it is experimentally supported that the higher modal frequencies show response to analytes. This data also experimentally support that mode frequency and not the mode order is responsible for the increased response.

8.3 Conclusions

In this chapter the effort on fabrication of polymer cantilevers is discussed. The motivation behind the idea of polymeric material for cantilevers is given. SU-8 photoepoxy polymer is chosen for polymer cantilever fabrication and the reasons are given and the other efforts for material selection are discussed in Section 8.1. The fabrication process for SU-8 cantilevers is discussed and successfully fabricated cantilevers images are shown. The Hg sensing data is presented for two different geometries of SU-8 levers.

The deflection response of the SU-8 cantilevers is found to be an order of magnitude larger than that of the Si cantilevers. Although a distinct spectral response is observed for these cantilevers, no promising shifts in the modal frequencies are observed upon Hg exposures. With further Hg studies of wider cantilevers, it is experimentally supported that sensing response can be obtained with thermal spectrum of SU-8 cantilevers and one needs to use the sixth order modal frequency at 620 kHz to get some sensing response. These are some preliminary studies that have been done on the SU-8 cantilevers and repetitions under different experimental conditions would help understand the promise of the thermal spectral studies of these cantilevers.

Chapter 9

CONCLUSIONS AND FUTURE WORK

The focus of this dissertation is to propose and demonstrate the use of thermally induced higher order cantilever modes for sensing applications. The use of the thermally induced cantilever spectrum is demonstrated for sensing applications with the Au-Hg system. The use of thermally induced higher order modes is also demonstrated to understand the adsorption related surface interactions with sputtered and thermally evaporated Au surfaces. Analytical techniques are employed to understand the higher order modal response to Hg with these two kinds of Au surfaces. Furthermore with the help of a new devised technique to end load cantilevers, it is shown that the higher order modes can be used for sensing with cantilevers having any Au coverage. To check if an increase in the number of flexural modes is observed with softer cantilevers, SU-8 cantilevers are fabricated. SU-8 cantilevers with similar geometry to the Si cantilevers studied here are studied for Hg response. An order of magnitude increase in the deflection signal is observed for SU-8 cantilevers, but no improvement in the spectral response is observed. However by using a wider SU-8 cantilever which showed more flexural modes in its spectrum, it is shown that with higher modal frequency, it is possible to see sensing response with SU-8 cantilevers. This also experimentally

supports that mode frequency not the mode order is responsible for the higher sensing response.

In this chapter, a summary of these studies pertaining to thermally induced higher order cantilever modes is presented and some future research plans follow.

9.1 Summary

After the basic concepts and experimental background are introduced (Chapter Two), the fabrication process for the Si cantilever is presented (Chapter Three). The process is successfully demonstrated by fabricating free standing straight Si cantilevers. The process has shown a yield of 66%. These cantilevers were not used throughout the studies presented in this dissertation for the reasons outlined in Chapter Three.

Using commercial rectangular Si cantilevers, the use of thermally induced higher order cantilever modes is demonstrated (Chapter Four). Detail analyses of the positions of the experimentally observed modes by various techniques confirmed that the experimentally observed modes are the flexural modes of cantilever vibrations. Comparison of the increase in the Q of the various modes with the literature revealed that the increase in the quality factor is limited by the support loss of the beam when using higher order modes. With fully loaded cantilevers, it is shown that the thermally induced higher order modes are more sensitive than the thermally induced fundamental mode for sensing Hg. A new yet simple technique to end load cantilevers is presented, and it is shown that the higher order modes respond to Hg when cantilevers are end loaded with Au using this technique.

A study of as deposited sputtered and thermally evaporated Au film surfaces used for Hg adsorption with cantilevers follows (Chapter Five). The two kinds of surfaces are

extensively studied with SEM and AFM before and after Hg exposures. The thermally induced spectral studies of cantilevers revealed that the surface morphology of the Au film plays an important role in modifying the flexural frequencies of the cantilever vibrations. The deflection response, however, does not show the effect of local morphological changes but only reflects the resultant stress associated with the Hg adsorption process. Thus it is concluded that as deposited sputtered films are more sensitive to Hg exposures than as deposited thermally evaporated films when studied using thermally induced higher order modes of cantilever vibration. This conclusion is further supported by studying cantilever spectral response as a function of % Au coverage with sputter deposited and thermally evaporated Au films.

In order to understand the Au surfaces in detail after the Hg exposures, a variety of analytical tools are used (Chapter Six). To explain the differences observed in the Hg spectral response of sputtered and thermally evaporated films, SEM and AFM studies proved to be helpful. To compare the crystallinity of the two Au film surfaces, XRD studies are carried out. To know the amount of Hg on the Au surface and its depth of penetration, EDS and XPS studies are carried out. The results obtained with these tools show that Hg is responsible for the nature of spectral shifts observed experimentally.

Study of the thermally induced flexural spectrum of rectangular Si cantilever with respect to percent Au coverage is presented (Chapter Seven). The motivations behind this study are presented along with its implications. The results of the study are presented and a simple explanation is given to explain the data. However it is understood that a rigorous model is needed to understand the full potential this data holds. Due to the novelty and

potential associated with this study, it is presented here as a chapter; however, it is also acknowledged that this chapter does not give complete insight into the data presented.

To check for possible improvement in the spectral sensing response, SU-8 cantilevers are fabricated. Full spectral characteristics of SU-8 cantilevers are extracted; however, the instability of the peaks is larger than expected. Although an order of magnitude increase is observed for the deflection signal of the SU-8 cantilevers, no improvement in the spectral response is observed. It is shown that with a wider SU-8 cantilever, it is possible to get Hg sensing response with thermally induced higher order modes. However further research is needed to get an optimized SU-8 cantilever for thermal spectrum studies.

9.2 Future Research

The work presented in this dissertation is mainly focused on the experimental study of thermally induced flexural modes of cantilever vibrations. The next efforts should be focused on (1) developing a theoretical model to understand the nature of spectral behavior as a function of the % Au coverage and (2) improving the thermal spectral response of SU-8 cantilevers and studying possible improvement in the sensing response of the higher order SU-8 cantilever modes.

9.2.1 Development of a Model to Understand the Spectral Behavior as a Function of % Au Coverage

As an initial investigation in understanding how a cantilever's mechanical properties (mainly its spring constant) change, spectral behavior of cantilevers has been

studied when the sensitizing coating percentage is varied. Thermally induced spectral response of the same cantilevers with different % Au coverage is noted.

Future research is needed to develop a rigorous model to understand this spectral response. As indicated from the study, the higher order modes show a continuous decrease in the frequency, however, with two different slopes. The fundamental mode does not show any change in its frequency after 20% Au coverage at the tip of the cantilever. Since this mode is widely used for mass sensing, understanding this behavior is important in order to say that, for the fundamental mode, the spring constant change is dominant for the cantilevers coated with sensitizing coating along the entire length except at the tip. A model where the mode shape, modal mass and the position of the Au strip with respect to the nodes and antinodes of various modes should be designed and solved to successfully understand the contributions of mass and stiffness matrices in the final spectral response. This theoretical result should be compared with the experimental data presented in Chapter 7 to establish a correlation which will tremendously help the cantilever research community to understand the mechanical behavior of cantilevers.

9.2.2 Improvement in the SU-8 Cantilevers Thermal Spectral Response

An order of magnitude improvement in the deflection response of SU-8 cantilevers presented in this dissertation is very promising. Given the poor thermal conductivity of the polymer matrix, the presence and extraction of the full spectral characteristic of these cantilevers is encouraging. However the standard deviation associated with the various thermally induced modes should be brought down to an acceptable value for their potential use in sensing. This can be done by various techniques, for example, by optimizing the cantilever geometry or by fabricating a local

heater to resistively heat the cantilever to increase the vibrational amplitude which may lead to an increase in Q and stability of the frequency position.

Not only do the frequency positions of SU-8 cantilevers need to be stabilized, but also the number of modes seen in their spectrum. This can be done by studying the different geometries of already fabricated SU-8 levers to understand which geometry gives the richest spectral response. Such cantilever geometry should then be further optimized so that the standard deviation of the various peaks is within an acceptable noise level. The spectral response of these optimized cantilevers to Hg would then be able to reveal the potential this approach has.

APPENDIX

FABRICATION PROCESS DETAILS

The purpose of this appendix is to give the detailed process steps involved in Si and SU-8 cantilever fabrication. Here the detailed die information related to the cantilever definition mask (Mask 1) is also given.

A.1 Si Cantilever Fabrication Process

1. Sputter deposition of 750nm of SiO2, RF power 200W, 5mT Ar.

2. Dehydration bake of the wafer 120^{o}C/30m.

3. HMDS vapor prime of top side for 15m.

4. Spin & bake i-line resist on top side 500rpm/100r/s/5s, 4000rpm/500r/s/60s & 90^{o}C/45sec.

5. HMDS vapor prime the bottom side for 15m.

6. Spin & bake i-line resist on bottom side 500rpm/100r/s/5s, 4000 rpm /500 r/s /60s & 90^{o}C/60sec.

7. Sandwich the wafer in the fixture Place wafer top side up on the fixture so that you can see the flat in the open bottom window of the top mask plate.

8. Expose top side 90 mJ/cm^{2}.

9. Expose bottom side 90mJ/cm^{2}.

10. Develop 1m in 9:1 AZ400:H_2O.

11. Develop inspect with optical microscope.

12. Sputter deposition of 50nm Cr on both sides 200W DC, 5mT Ar, 90s Top first then bottom side.

13. Liftoff with acetone for 1m in ultrasonic agitator.

14. Dehydration bake Bottom side at 120^{o}C/30m.

15. HMDS vapor prime for 15m.

16. Spin and Bake i-line resist, 500rpm/100r/s/5s,4000rpm/500r/s/60s 90^{o}C/1m.

17. Align kays1 to Mask1 target alignment marks, make sure all the four keys are aligned by the same amount.

18. Expose w Mask1, 90mJ/cm^2.

19. Develop for 1m in 9:1 AZ400:H_2O.

20. Develop Inspect, both under optical microscope and P-10 profiler.

21. Si Etch, 40sccm SF6, 5 sccm O2, 150W, 75mT Sietch.prc in RIE 4:15m.

22. Etch Inspect with P-10 profiler.

23. Resist Stripoff in acetone bath 2m, IPA rinse, N2 dry, 10m in oven.

24. Etch Inspect with p-10 and optical microscope.

25. Spin PI2616 at 500rpm/50r/s/10s, 5000rpm/500r/s/60s LANL recipe.

26. Cure PI2525 furnace cure LANL recipe.

27. Protect Inspect with optical microscope.

28. HMDS vapor prime for 15m.

29. Spin & bake i-line resist, 500rpm/100r/s/5s,4000rpm/500r/s/60s 90^oC/1m.

30. Align kays3 to Mask3 target alignment marks, make sure all the four keys are aligned by the same amount.

31. Expose w Mask3, 90mJ/cm^2.

32. Develop for 1m in 9:1 AZ400:H_2O.

33. Develop Inspect.

34. BOE etch of 1μm SiO2, 315nm/m for sputtered oxide.

35. Etch Inspect with P-10 profiler.

36. Resist Stripoff in acetone bath 2m, IPA rinse, N2 dry, 10m in oven.

37. Stripoff inspect with P-10 profiler.

38. Dehydration Bake at 120^oC/30m.

39. HMDS vapor prime 15m.

40. Spin 1075, Edge Bead Removal (EBR), 500rpm/100r/s/5s, 4000rpm/500r/s/70s EBR 100/10/60,

41. Bake 1075 at 100^{o}C/3m hotplate.

42. Inspect for uniformity and defects.

43. Align kays2 to Mask2 target alignment marks, make sure all the four keys are aligned by the same amount.

44. Expose with Mask2 for 150s.

45. Develop for 10m in the tall container, 45s ultrasonic, 5m in the tall container.

46. Develop Inspect with P-10 profiler.

47. Hardbake at 115^{o}C/45m on hotplate.

48. Delay etch the 50μm tabs at Auburn with ICP-RIE and the Bosche process with C_4F_8, SF_6 and O_2 chemistry.

49. BOE etch 750nm SiO_2.

50. Deep etch the entire wafer at Auburn with ICP-RIE and the Bosche process with C_4F_8, SF_6 and O_2 chemistry.

51. Etch inspect with optical microscope for alignment between mask 2 and 3.

52. Release handle wafer from sample wafer by acetone soak for 4hrs then take sample wafer out.

53. IPA soak for 2Hrs, let it sit and dry. NO N_2 gun.

54. BOE etch the 750nm oxide.

55. Ash PI with O2descum.prc recipe in RIE, 40sccm O2, 100W, 10mT, 30m.

A. 2 Mask 1 Die Information

The die numbering and cantilever geometry information related to Mask 1 is as follows. The placement of different dies on a fabricated SOI wafer is as shown in Figure A.1. The related numbering is as shown in Figure A.2 and the cantilever geometry information is given in Table A.1.

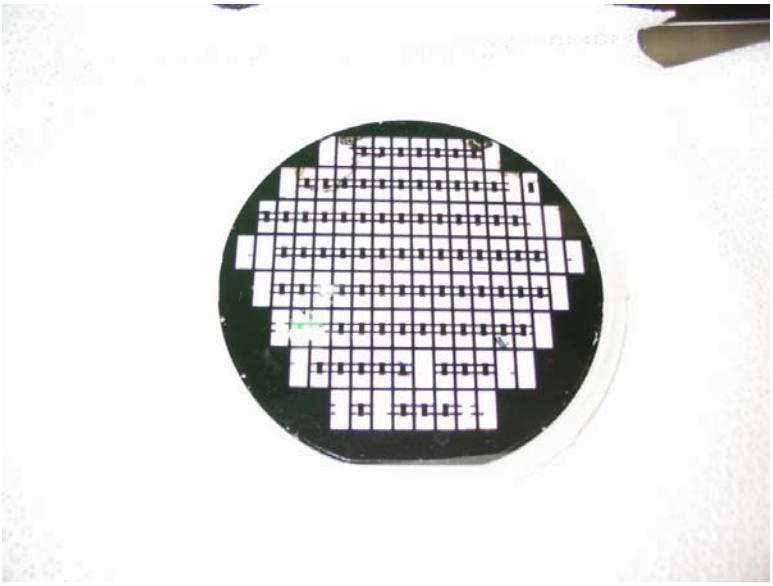

Figure A.1 SOI wafer after completion of the whole fabrication process. Each rectangular block holds one cantilever die

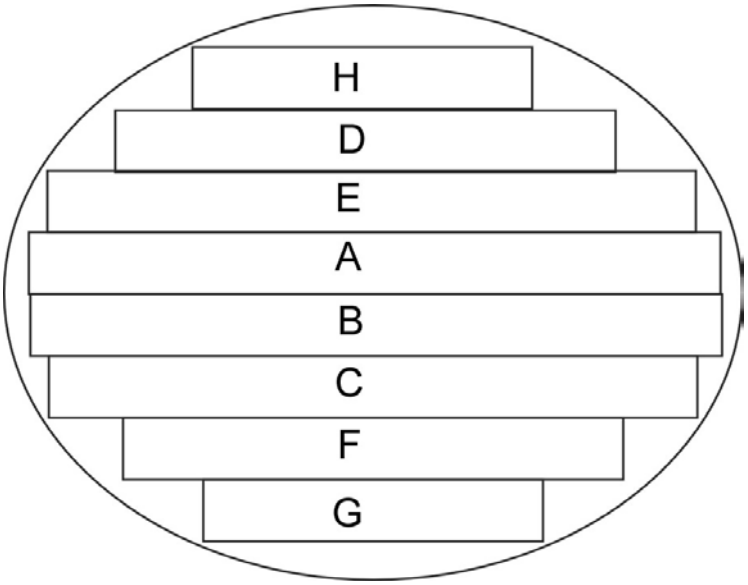

Figure A.2 Numbering on Mask 1 for the 4” SOI wafer

Table A.1 Cantilever geometry information related to Mask1.

Die Symbol used in the TLC file	Lever length on one side of the die (um)	Lever length on other side of the die (um)	Lever Width (um)	# of lever per die	Row # on the mask
H	100	100	35	2	1
D	300	100	100	6	2
E	250	150	35	6	3
A	300	100	35	6	4
B	300	200	35	6	5
C	200	100	35	6	6
F	300	300	35	2	7
G	200	200	35	2	8

A.3 SU-8 Cantilever Fabrication Process

1. 5nm Cr/50nm Au/50nm Cr Deposition with DC sputtering.

2. Alignment marks transfer
    1. Dehydration bake at 90^{o}C/15m/white oven.
    2. HMDS vapor prime for 15m.
    3. Spin i-line resist 4000rpm/500r/s/60s.
    4. Softbake the resist at 90^{o}C/1m/hotplate.
    5. Expose through Top sandwich mask Mask5 for 90mJ/cm^{2}.
    6. Develop for 1m.
    7. Observe with optical microscope.
    8. 50nm Au deposition with sputtering.
    9. Liftoff in Acetone with ultrasonic agitation for 1m.

3. Microcantilever Definition
    1. Spin SU-8 2001 500rpm/50r/s/5s, 2500rpm/500r/s/50s.
    2. Softbake SU-8 2001 at 65^{o}C/1m, 95^{o}C/1m.
    3. Expose through Mask1-SU8 for 90mJ/cm^{2}.
    4. Post exposure bake at 65^{o}C/1m, 95^{o}C/1m.
    5. Develop for 1m.
    6. Rinse in IPA and N_2 dry.

4. Die Definition
    1. Spin SU-8 2100 at 500rpm/50r/s/10s, 1000rpm/100r/s/60s.
    2. Softbake SU-8 2100 at 65^{o}C/15m, 95^{o}C/35m.
    3. Expose through Mask2 for 260s.
    4. Pose exposure bake at 65^{o}C/1m, 95^{o}C/15m.

5. Develop for 15m with ultrasonic agitation.
6. Rinse in IPA and N_2 dry.
7. Hardbake at 65^{o}C/1m, 95^{o}C/5m, 195^{o}C/15m on hotplate.

5. Release
    1. Wet Cr etch for 15m.
    2. Rinse with Water and N_2 dry.

REFERENCES

[1] S. Middelhoek, Sens. and Actua. A, **41**(1-3), 1, (1994)

[2] R. Berger, Ch. Gerber, H.P. Lang and J.K. Gimzewski, Microelectronic Eng., **35**(1-4), 373, (1997)

[3] A. Boisen, J. Thaysen, H. Jensenius and O. Hansen, Ultramicroscopy, **82**(1-4), 11, (2000)

[4] B.H. Kim, F.E. Prins, D.P. Kern, S. Raible and U. Weimar, Sens. and Actua. B, **78**(1-3), 12, (2001)

[5] D. Lange, C. Hagleitner, O. Brand and H. Baltes, Micro Electro Mechanical Systems, 2001. MEMS 2001, the 14th IEEE International Conference on, 547, (2001)

[6] A. Hammiche, L. Bozec, M. Conroy, H.M. Pollock, G. Mills, J.M.R.Weaver, D.M. Price, M. Reading, D.J. Hourston and M. Song, J. Vac. Sci. and Tech. B, **18**(3), 1322, (2000)

[7] T. Lalinsky, E. Burian, M. Drzik, S. Hascik, Z. Mozolova and J. Kuzmik, J. Micromech. and Microeng., **10**, 293, (2000)

[8] K.B. Brown, W. Allegretto, F.E. Vermuelen, R.P.W. Lawson and A.M. Robinson, Electrical and Computer Engineering, 1999 IEEE Canadian Conference on, 3, 1686, vol.3, (1999)

[9] M. Zaborowski, P. Grabiec, T. Gotszalk, E. Romanowska and I.W. Rangelow, Microelectronic Eng., **57-58**, 787, (2001)

[10] D.R. Baselt, G.U. Lee, K.M. Hansen, L.A. Chrisey and R.L. Colton, Proceedings of the IEEE, **85**(4), 672, (1997)

[11] T. Sulchek, R. Hsieh, S.C. Minne, C.F. Quate and S.R. Manalis, IEEE-NANO 2001, Proceedings of the 2001 1st IEEE Conference on, 562, (2001)

[12] P. A. Arutyunov and A. L. Tolstikhina, Measurement Techniques, **45**(7), 714, (2002)

[13] Masami Kageshima, Hisato Ogiso, Shizuka Nakano, Mark A. Lantz and Hiroshi Tokumoto, Japanese J. Appl. Phys., **38**(6), 3958, (1999)

[14] G. Binning, C. Gerber, E. Stoll, T.R. Albrecht and C.F. Quate, Surface Science, **189-190**, 1, (1987)

[15] D. Sarid, Scanning Force Microscopy. Oxford University Press

[16] R. Wiesendanger, Scanning Probe Microscopy and Spectroscopy. Cambridge University Press, (1994)

[17] S.J. O'Shea, M.E. Welland, T.A. Brunt, A.R. Ramadan and T. Rayment, J. Vac. Sci. Tech. B, **14**(2), 1383, (1996)

[18] T. Thundat, S. L. Sharp, W. G. Fisher, R. J. Warmack and E. A. Wachter, Appl. Phys. Letts., **66**(12), 1563, (1995)

[19] M. K. Baller, H. P. Lang, J. Fritz, Ch. Gerber, J. K. Gimzewski, U. Drechsler, H. Rothuizen, M. Despont, P. Vettiger, F. M. Battiston, J. P. Ramseyer, P. Fornaro, E. Meyer and H.-J. Guntherodt, Ultramicroscopy, **82**(1-4), 1, (2000)

[20] R. Berger, E. Delamarche, H. P. Lang, C. Gerber, J. K. Gimzewski, E. Meyer and H. J. Guentherodt, Appl. Phys. A, **66**(1-2), S55, (1998)

[21] S. J. O'Shea, M. E. Welland, T. A. Brunt, A. R. Ramadan and T. Rayment, J. Vac. Sci. Tech. B, **14**(2), 1383, (1996)

[22] T. A. Brunt, E. D. Chabala, T. Rayment, S. J. O'Shea and M. E. Welland, J. Chem. Soc.-Faraday Transactions, **92**(20) 3807, (1996)

[23] J. Fritz, M. K. Baler, H. P. Lang, H. Rothuizen, P. Vettiger, E. Meyer, H.-J. Guntherodth, Ch. Gerber and J. K. Gimzewski, Science, **288**(5464), 316, (2000)

[24] Guanghua Wu, Haifeng Ji, Karolyn Hansen, Thomas Thundat, Ram Datar, Richard Cote, Michael F. Hagan, Arup K. Chakraborty and Arunava Majumdar, Proceedings of the National Academy of Sciences of the USA, **98**(4), 1560, (2001)

[25] J. K. Gimzewski, Ch. Gerber, E. Meyer and R. R. Schlittler, Chem. Phys. Letts., **217**(5-6), 589, (1994)

[26] J.E. Sader, J. Appl. Phys., **89**(5), 2911, (2001)

[27] H. Baltes, A. Koll and D. Lange, ISIE '97, Proceedings of the IEEE International Symposium on Industrial Electronics, vol.1 (Cat.No.97^{TH}8280), SS152, (1997)

[28] C. Hagleitner, A. Hierlemann, D. Lange, A. Kummer, N. Kerness, O. Brand and H. Baltes, Nature, **414**, 293, (2001)

[29] Y.T. Yang, K.L Ekinci, X.M.H. Huang, L.M. Schiavone and M.L. Roukes, Appl. Phys. Letts., **78**(2), 162, (2001)

[30] A.N. Cleland and M.L. Roukes, Appl. Phys. Letts., **69**(28), 2653, (1996)

[31] H.P. Lang, R. Berger, J.K. Gimzewski, P. Fornaro and E. Meyer, Anal. Chim. Acta, **393**(1-3), 59, (1999)

[32] H.P. Lang, R. Berger, F. Battiston, J.-P. Ramseyer, E. Meyer, C. Andreoli, J. Brugger, P. Vettiger, M. Despont, T. Mezzacasa, L. Scandella, H.-J. Guntherodt, C. Gerber and J.K. Gimzewski, Appl. Phys. A Materials Science, **66**(7), S61, (1998)

[33] M.L. Roukes, TRANSDUCERS '01. EUROSENSORS XV. 11th International Conference on Solid-State Sensors and Actuators. Digest of Technical Papers, 658 vol.1, (2001)

[34] T. Thundat, G.Y. Chen, R.J. Warmack, D.P. Allison and E.A. Wachter, Analytical Chemistry, **67**(3), 519, (1995)

[35] T. Thundat, E.A. Wachter, S.L. Sharp and R.J. Warmack, Appl. Phys. Letts., **66**(13), 1695, (1995)

[36] J. Yang, T. Ono and M. Esashi, Sens. and Actua., **82**, 102, (2000)

[37] T. Ono, X. Li, H. Miyashita and M. Esashi, Rev. Sci. Instru., **74**(3), 1240, (2003)

[38] Z.L. Wang and P. Poncharal W.A. de Heer, J. Phys. and Chem. of Solids, **61**, 1025, (2000)

[39] J.W.M. Chon, Paul Mulvaney and J.E. Sader, J. Appl. Phys., **87**(8), 3978, (2000)

[40] J.E. Sader, J. Appl. Phys., **84**(1), 64, (1998)

[41] Rachel McKendry, Jiayun Zhang, Youri Arntz, Torsten Strunz, Martin Hegner, Hans Peter Lang, Marko K Baller, Ulrich Certa, Ernst Meyer, Hans-Joachim Guntherodt and Christoph Gerber, Proceedings of the National Academy of Sciences of the USA, **99**(15), 9783, (2002)

[42] K.M. Hansen, H.-F. Ji, G. Wu, R. Datar, R. Cote, A. Majumdar and T. Thundat Analytical Chemistry A, **73**(7), 1567, (2001)

[43] B. Ilic, D. Czaplewski, M. Zalalutdinov, H.G. Craighead, P. Neuzil, C. Campagnolo and C. Batt, J. Vac. Sci. Tech. B, **19**(6), 2825, (2001)

[44] N. Blanc, J. Brugger and N.F. de Rooij, J. Vac. Sci. Tech. B, **14**(2), 901, (1996)

[45] I. S. Chen, J.F. Roeder, D.J. Kim, J.P. Maria and A.I. Kingon, J. Vac. Sci. Tech. B, **19**(5), 1833, (2001)

[46] A.N. Cleland, M. Pophristic and I. Ferguson, Appl. Phys. Letts., **79**(13), 2070, (2001)

[47] J. Gaspar, V. Chu, N. Louro, R. Cabeca and J.P. Conde, J. of Non-Crystalline Solids, **299-302**, 1224, (2002)

[48] D.S. Greywall, B. Yurke, P.A. Busch and A.N. Pargellis, Phys. Rev. Letts., **72**(19), 2992, (1994)

[49] H.J. Cho and C.H. Ahn, MEMS 2000, The Thirteenth Annual International Conference on, 686, (2000)

[50] B. Yu, W. Allegretto and A.M. Robinson, Electrical and Computer Engineering, 1999 IEEE Canadian Conference on, 1643 vol.3, (1999)

[51] T. Goddenhenrich, H. Lemke, U. Hartmann and C. Heiden, J. Vac. Sci. Tech. A, **8**(1), 383, (1990)

[52] G. Neubauer, S.R. Cohen, G.M. McClelland, D. Horne and C.M. Mate, Rev. of Sci. Instru., **61**(9), 2296, (1990)

[53] M. Madou, Fundamentals of Microfabrication, CRC Press LLC, (1997)

[54] S.M. Sze, Semiconductor Devices, Physics and Technology. Bell Telephone Laboratories, Inc., (1985)

[55] J. Thaysen, A. Boisen, O. Hansen and S. Bouwstra, Sens. and Actua. B, **83,** 47, (2000)

[56] P. Rasmussen, J. Thaysen, S. Bouwstra and A. Boisen, Sens. and Actua. A, **92**, 96, (2001)

[57] Y. Su, A.G.R. Evans, A. Brunnschweiler and G. Ensell, J. of Micromech. and Microeng., **12**, 780, (2002)

[58] Y. Su, A.G.R. Evans and A. Brunnschweiler, J. of Micromech. and Microeng., **6**, 69, (1996)

[59] J. Thaysen, A.D. Yalcinkaya, R.K. Vestergaard, S. Jensen, M.W. Mortensen, P.Vettiger and A. Menon, Technical Digest of MEMS 2002, (CatNo.0780371852) 320, (2002)

[60] R.P. Ried, H.J. Mamin, B.D. Terris, Long-Sheng Fan and D. Rugar. J. of Microelectromechanical Systems, **6**(4), 294, (1997)

[61] T. E. Schaffer and H. Fuchs, J. Appl. Phys., **97**, 083524, (2005)

[62] R. Sandberg, W. Svendsen, K. Molhave and A. Boisen, J. Micromech. Microeng., **15**, 1454, (2005)

[63] F. Lochon, I. Dufour and D. Rebiere, Sens. Actua., B **108**, 979, (2005)

[64] Z. Hao, A. Erbil and F. Ayazi, Sens. Actua., A **109**, 156, (2003)

[65] L. B. Sharos, A. Raman, S. Crittenden, and R. Reifenberger, Appl. Phys. Lett., 84, 4638, (2004)

[66] T. Thundat, E. A. Wachter, S. L. Sharp and R. J. Warmack, Appl. Phys. Lett., **66**, 1695, (1995)

[67] T. Thundat, FL J. Warmack, G. Y. Chen and D. P. Allison, Appl. Phys. Lett., **64** (21), 2894, (1994)

[68] E. A. Wachter and T. Thundat, Rev. Sci. Instru., **66**, 3662, (1995)

[69] Z. Hu, T. Thundat and R. Warmach, J. Appl. Phys., **90**, 427, (2001)

[70] B. Rogers, L. Manning, M. Jones, T. Sulchek, K. Murray, B. Beneschott, J. Adams, Z. Hu, T. Thundat, H. Cavazos and S. Minne, Rev. Sci. Instru., **74**, 4899, (2003)

[71] J. P. Cleveland, S. Manne, D. Boceka and P. K. Hansma, Rev. Sci. Instru., **64**, 403 (1993)

[72] J. L. Hutter and J. Bechhoefer, Rev. Sci. Instru., **64**, 1868 (1993)

[73] H-J. Butt and M. Jaschke, Natotechnology, **6** (1995)

[74] S. Cherian and T. Thundat, Appl. Phys. Lett., **80**, 2219, (2002)

[75] M. Godin, V. Tabard-Cossa and P. Grutter, Appl. Phys. Lett., **79**, 551, (2001)

[76] A. W. McFarland, M. Poggi, M. J. Doyle, L. A. Bottomley and J. S. Colton, Appl. Phys. Lett., **87**, 053505, (2005)

[77] J. Yang, T. Ono and M. Esashi, J. Vac. Sci. Technol. B, **19**, 551, (2001)

[78] K. Y. Yasumura, T. D. Stowe, E. M. Chow, T. Pfafman, T. W. Kenny and D. Rugar, Proceedings of the Solid-State Sensor and Actuator Workshop, Hilton Head Island, South Carolina, 8-11, 65, (1998)

[79] Y. J. Wright, A. K. Kar, Y. W. Kim, C. Scholz and M. A. George, Sens. Actua. B, **107**, 242 (2004)

[80] M. V. Salapaka, H. S. Bergh, J. Lai, A. Majumdar and E. McFarland, J. Appl. Phys., **81**, 2480 (1997)

[81] A. K. Kar and M. A. George, J. Appl. Phys, **94**(7), 4626, (2003)

[82] A. R. Kadam, G. P. Nordin and M. A. George, J. Appl. Plys., Accepted for publication.

[83] J. E. Sader, I. Larson, P. Mulvaney and L. R. White, Rev. Sci. Instrum., **66**, 3789 (1995)

[84] P. I. Oden, Sens. Actua. B, **53**, 191 (1998)

[85] A. R. Kadam, M. A. George and G. P. Nordin, J. Vac. Sci. Tech. B, submitted Apr 06.

[86] Yung-Chun Lee, Jhih-Ming Yu and Shiang-Wen Huang, Key Eng. Maters., **270-273**, 1406, (2004)

[87] Xuefeng Wang, Jonathan Engel and Chang Liu, J. Micromech. Microeng., **13,** 628, (2003)

[88] G. Genolet, J. Brugger, M. Despont, U. Drechsler, P. Vettiger, N. F. Rooij and D. Anselmetti, Rev. Sci. Instrum. **70,** 2398, **(**1999)

[89] J. Thaysen, A. D. Yalcinkaya, P. Vettiger and A. Menon, J. Phys. D, **35** 2698, (2002)

[90] A. Johansson, M. Calleja, P.A. Rasmussen and A. Boisen, Sens and Actua. A, **123–124** 111, (2005)

[91] M. Calleja, M. Nordstrom, M. Alvarez, J. Tamayo, L.M. Lechuga and A. Boisen, Ultramicroscopy, **105**(1-4), 215, (2005)

[92] C. Battistoni, E. Bemporad, A. Galdikas, S. Kaciulis, G. Mattogno, S. Mickevieius and V. Olevano, Appl. Surf. Sci, **103**, 107, (1996)

[93] T. Kobiela, B. Nowakowski and R. Dus, Appl. Surf. Sci, **206**, 78, (2003)